The Imaginary Universe (on the Three Complementary Sets of Measurement Units Defining Three Dark Electrons)

Szymon Łukaszyk *

Posted Date: 28 August 2024

doi: 10.20944/preprints202212.0045.v20

Keywords: emergent dimensionality; fine-structure constant; Planck units; dark quantum states, gravitational observations; holographic principle; mathematical physics

 doi:10.20944/preprints202212.0045.v20

Article

The Imaginary Universe (On the Three Complementary Sets of Measurement Units Defining Three Dark Electrons)

Szymon Łukaszyk

Łukaszyk Patent Attorneys, ul. Głowackiego 8, 40-052 Katowice, Poland; szymon@patent.pl

Abstract: Three Fresnel coefficients for the normal incidence of electromagnetic radiation on monolayer graphene establish three complementary fine-structure constants, two of which are negative. Each introduces its own specific set of Planck units. Hence, two sets of basic Planck units are real and two are imaginary. The elementary charge is the same in all those sets of Planck units, establishing equality between the products of each fine-structure constant and the speed of light it is associated with, and defining the dark electron in each of these three complementary systems. All fine-structure constants are related to each other through the constant of π, which indicates that they do not vary over time. The negative complementary fine-structure constant established by the graphene reflectance is dual to the fine-structure constant. The assumption of universality of the black hole entropy formula to the remaining two stellar *objects* emitting perfect black-body radiation less dense than a black hole (neutron stars and white dwarfs) renders their energies exceeding their mass-energy equivalence. To accommodate this unphysical result, we introduced an imaginary mass and defined three complex energies in terms of real and imaginary Planck units, storing the surplus energy in their imaginary parts. It follows that black holes are fundamentally uncharged and have a vanishing imaginary mass. We have derived the lower bound on the mass of a charged black-body *object*, the upper bound on a white dwarf radius, and the equilibrium density of all three complex energies. The complex force between real masses and imaginary charges leads to the complex black-body *object's* surface gravity and generalized Hawking radiation complex temperature. Furthermore, based on the Bohr model for the hydrogen atom, we show that complex conjugates of this force represent atoms and antiatoms. The proposed model considers the value(s) of the fine-structure constant(s), which is(are) otherwise neglected in general relativity, and explains the registered (GWOSC) high masses of neutron star mergers and the associated fast radio bursts (CHIME) without resorting to any hypothetical types of exotic stellar *objects*.

Keywords: emergent dimensionality; fine-structure constant; Planck units; dark quantum states; gravitational observations; holographic principle; mathematical physics

---

1. Introduction

The universe began with the Big Bang, a prevailing scientific opinion. However, this Big Bang was not an explosion of 4-dimensional spacetime, which is also a current prevailing scientific opinion, but an explosion of dimensions that started in (-1)-dimensional void. The only exception to the general formula for the integral of a volume unit a^n, where a is the length of an edge in any dimension n is $n = -1$, where a jump discontinuity occurs and $\int a^{-1} da = \ln(a)$. A first 0-dimensional point appeared in the (-1)-dimensional void, inducing the appearance of other points that were indistinguishable from the first. The breach made by the first operation of the *dimensional successor function* of the Peano axioms inevitably continued leading to the formation of 1-dimensional, real and imaginary lines, allowing for an ordering of points using multipliers of real units (ones) or imaginary units ($a \in \mathbb{R} \Leftrightarrow a = 1b$, and $a \in \mathbb{I} \Leftrightarrow a = ib$, where $b \in \mathbb{R}$). Then, out of the two lines of each kind, crossing each other only at one initial point $(0, 0)$, the dimensional successor function formed 2-dimensional $\mathbb{R}^2$, $\mathbb{I}^2$, and $\mathbb{R} \times \mathbb{I}$ Euclidean planes, with $\mathbb{I}^2$ being a mirror reflection of $\mathbb{R}^2$. Thus, forming n-dimensional

 doi:10.20944/preprints202212.0045.v20

Euclidean spaces $\mathbb{R}^a \times \mathbb{I}^b$ with $a \in \mathbb{N}$ real and $b \in \mathbb{N}$ imaginary lines, $n = a + ib$, and the scalar product defined by

$$\mathbf{x} \cdot \mathbf{y} = \left(x_1, \ldots, x_a, ix'_1, \ldots, ix'_b\right)\left(y_1, \ldots, y_a, iy'_1, \ldots, iy'_b\right) := \sum_{k=1}^{a} x_k y_k + \sum_{l=1}^{b} x'_l \overline{y'_l}, \tag{1}$$

where $\mathbf{x}, \mathbf{y} \in \mathbb{R}^a \times \mathbb{I}^b$. With the appearance of the first 0-dimensional point, information has begun to evolve [1–9], initially using undirected exploration in a selectionless [8] and a timeless [9] assembly process.

Mathematics is theoretically infinite, so determining why some math corresponds to our observable universe and the rest does not is a highly nontrivial problem [10]. Fortunately, the mathematical properties of particular dimensions are not the same. For regular convex n-polytopes, for example, there are countably infinitely many regular convex polygons, five regular convex polyhedra (Platonic solids), six regular convex 4-polytopes and only three regular convex n-polytopes if $|n| > 4$ and $|n| < 0$ [11]. In particular, a 4-dimensional Euclidean space is endowed with a peculiar property known as exotic $\mathbb{R}^4$ [12], absent in other dimensionalities. Owing to this property, $\mathbb{R}^3 \times \mathbb{I}$ Euclidean space provides a continuum of homeomorphic but non-diffeomorphic differentiable structures and this is necessary for biological evolution, as it allows the variation of phenotypic traits within populations of individuals [13]: each piece of individually memorized information is homeomorphic to the corresponding piece of individually perceived information but remains non-diffeomorphic (non-smooth). Hence, selection [8] and time [9] emerged and the evolution of information had to inevitably exploit directed exploration provided by biological evolution. Exotic $\mathbb{R}^4$ solves the problem of extra dimensions of nature, and perception requires a natural number of (thus independent) dimensions to form perceived space [14]. Each biological cell and each biological agent perceives an emergent space of three real dimensions and one imaginary (time) observer-dependently [15] and at present, when $i0 = 0$ is *real*, through a spherical Planck triangle corresponding to one bit of information in units of $-c^2$, where c is the speed of light in vacuum. This is the principle of emergent dimensionality (ED) [5,6,9,13,16,17].

Human perception involves measuring and measuring requires measurement units. In 1899 Max Planck derived the *natural* units of measure as "independent of special *bodies* or *substances*, thereby necessarily retaining their meaning for all times and for all civilizations, including extraterrestrial and nonhuman ones" [18]. Planck units utilize the Planck constant h introduced in his black-body radiation formula. Earlier, in 1881, George Stoney derived a system of natural units [19] based on the elementary charge e (Planck's constant was unknown at this time). The ratio of Stoney units to Planck units is $\sqrt{\alpha}$, where α is the fine-structure constant. This study derives three complementary sets of Planck units based on the three complementary fine-structure constants established by the Fresnel coefficients for the normal incidence of electromagnetic radiation on monolayer graphene (MLG) and hints at certain areas of their applicability. We chose Planck units over other natural unit systems not only because they incorporate the fine-structure constant α and the Planck constant h. Other systems of natural units (except for Stoney units) also incorporate them. This is because only the Planck area defines one bit of information on a patternless black hole surface given by the Bekenstein bound (52) and the binary entropy variation [5,6].

The paper is organized as follows. Section 2 shows that the Fresnel coefficients for the normal incidence of electromagnetic radiation on MLG include three complementary fine-structure constants, including two negative ones and hinting that the negative complementary fine-structure constant α_2 established by the graphene reflectance is dual to the fine-structure constant α. Section 3 presents complementary sets of α_*-Planck units established by these three fine-structure constants. Section 4 introduces the concept of a black-body *object* in thermodynamic equilibrium that emits perfect black-body radiation and reviews its necessary properties. Section 5 introduces complex energies expressed in terms of real and imaginary α_--Planck units and applies them to black-body *objects* to show that in this model α and α_2 are indeed dual to each other. Section 6 defines complex forces

 doi:10.20944/preprints202212.0045.v20

based on the products of the complex energies. The complex force between real masses and imaginary charges is applied in Section 7 to the Bohr model of the hydrogen atom and in Section 8 to derive a black-body *object* surface gravity and the generalized Hawking radiation temperature. Section 9 considers the observed mergers of black-body *objects* to show that the observed data can be explained without the need to introduce hypothetical exotic stellar *objects*. Section 10 discusses fluctuations of black-body *objects*. Section 11 summarizes the findings of this study.

2. Three Complementary Fine-Structure Constants

Numerous publications provide Fresnel coefficients for the normal incidence of electromagnetic radiation (EMR) on monolayer graphene (MLG), which are remarkably defined only by π and the fine-structure constant α having the inverse

$$\alpha^{-1} = \left(\frac{q_{\mathrm{P}}}{e}\right)^2 = \frac{4\pi\epsilon_0\hbar c}{e^2} \approx 137.036, \tag{2}$$

where q_{P} is the Planck charge, $\hbar$ is the reduced Planck constant, $\epsilon_0 \approx 8.8542 \times 10^{-12}$ $[\mathrm{kg}^{-1} \cdot \mathrm{m}^{-3} \cdot \mathrm{s}^2 \cdot \mathrm{C}^2]$ is the vacuum permittivity (electric constant), and e is the elementary charge. We choose this set of units over $[\mathrm{F{\cdot}m}^{-1}]$ for ϵ_0, since the mass, length, time, and charge units can express all the electrical units and together with temperature, amount of substance, and luminous intensity, these are the base units of the International System of Quantities (ISQ). Furthermore, in this notation we see that ϵ_0 is dependent on the unit of time. Transmittance (T) of MLG

$$\mathrm{T} = \frac{1}{\left(1 + \frac{\pi\alpha}{2}\right)^2} \approx 0.9775, \tag{3}$$

for normal EMR incidence was derived from the Fresnel equation in the thin-film limit [20] (Eq. 3), whereas a spectrally flat absorptance (A) $\mathrm{A} \approx \pi\alpha \approx 2.3\%$ has been reported [21,22] for photon energies between approximately 0.8011×10^{-19} and 4.0054×10^{-19} [J]. T is related to reflectance (R) [23] (Eq. 53) as $\mathrm{R} = \pi^2\alpha^2\mathrm{T}/4$, i.e,

$$\mathrm{R} = \frac{\frac{1}{4}\pi^2\alpha^2}{\left(1 + \frac{\pi\alpha}{2}\right)^2} \approx 1.2843 \times 10^{-4}, \tag{4}$$

The above equations for T and R, as well as the equation for the absorptance

$$\mathrm{A} = \frac{\pi\alpha}{\left(1 + \frac{\pi\alpha}{2}\right)^2} \approx 0.0224, \tag{5}$$

were also derived [24] (Eqs. 29-31) based on the thin-film model (setting $n_s = 1$ for the substrate). The sum of the transmittance (3) and reflectance (4) at normal EMR incidence on the MLG was derived [25] (Eq. 4a) as

$$\mathrm{T} + \mathrm{R} = 1 - \frac{4\sigma\eta}{4 + 4\sigma\eta + \sigma^2\eta^2 + k^2\chi^2} = \frac{1 + \frac{1}{4}\pi^2\alpha^2}{\left(1 + \frac{\pi\alpha}{2}\right)^2} \approx 0.9776, \tag{6}$$

where $\eta \approx 376.73$ $[\mathrm{kg} \cdot \mathrm{m}^2 \cdot \mathrm{s} \cdot \mathrm{C}^{-2}]$ is the vacuum impedance, $\sigma = e^2/(4\hbar) = \pi\alpha/\eta \approx 6.0853 \times 10^{-5}$ $[\mathrm{kg}^{-1} \cdot \mathrm{m}^{-2} \cdot \mathrm{s}^{-1} \cdot \mathrm{C}^2]$ is the MLG conductivity [26], k is the wave vector of light in vacuum, and $\chi = 0$ is the electric susceptibility of vacuum. Therefore, these coefficients are well established both theoretically and experimentally [20–22,25,27,28].

As a consequence of the conservation of energy

$$\mathrm{R} + (\mathrm{T} + \mathrm{A}) = 1. \tag{7}$$

In other words, the transmittance in the Fresnel equation describing the reflection and transmission of EMR at normal incidence on a boundary between different optical media is, in the case of the

 doi:10.20944/preprints202212.0045.v20

2-dimensional (boundary) MLG, modified to include its absorption (cf. Appendix C). Furthermore, $\sqrt{\mathrm{R}}+\sqrt{\mathrm{T}}=1$ and $\mathrm{A}=2\sqrt{\mathrm{RT}}$. Notably for Fresnel coefficients (A12) (cf. Appendix C), $\sqrt{\mathrm{R_F}}+\sqrt{\mathrm{T_F}}=1$ solves to $n_1=n_2$ which implies no refraction. We note that each conservation law is associated with a certain symmetry, as asserted by Noether's theorem. In this case, the symmetry involves the fine-structure constant α and π.

2.1. Reflectance

The reflectance $\mathrm{R}=0.013\%$ (4) of the MLG can be expressed as a quadratic equation of α

$$\mathrm{R}\Big(1+\frac{\pi\alpha}{2}\Big)^2-\frac{1}{4}\pi^2\alpha^2=0,\quad \frac{1}{4}(\mathrm{R}-1)\pi^2\alpha^2+\mathrm{R}\pi\alpha+\mathrm{R}=0, \tag{8}$$

which can be expressed in terms of the reciprocal of α, defining $\beta\coloneqq 1/\alpha$ as

$$\mathrm{R}\beta^2+\mathrm{R}\pi\beta+\frac{1}{4}(\mathrm{R}-1)\pi^2=\mathrm{R}\Big(\beta+\frac{\pi}{2}\Big)^2-\frac{\pi^2}{4}=0. \tag{9}$$

The quadratic equation (9) has two roots

$$\beta=\alpha^{-1}=\frac{-\pi\mathrm{R}+\pi\sqrt{\mathrm{R}}}{2\mathrm{R}}\approx 137.036,\quad \text{and} \tag{10}$$

$$\beta_2=\alpha_2^{-1}=\frac{-\pi\mathrm{R}-\pi\sqrt{\mathrm{R}}}{2\mathrm{R}}\approx -140.178. \tag{11}$$

Therefore, equation (8) includes the second negative fine-structure constant α_2. It turns out that the sum of the reciprocals of these fine-structure constants (10) and (11)

$$\alpha^{-1}+\alpha_2^{-1}=\frac{-\pi R+\pi\sqrt{\mathrm{R}}-\pi R-\pi\sqrt{\mathrm{R}}}{2\mathrm{R}}=\frac{-2\pi}{2}=-\pi,\quad \forall \mathrm{R}\neq 0, \tag{12}$$

is a transcendental number independent of the value of the reflectance R. Furthermore, the minimum of parabola (9) amounts $-\pi^2/4\approx -2.4674$ and occurs at $-\pi/2\approx -1.5708$, as shown in Figure 1. Also, these values are independent of the reflectance.

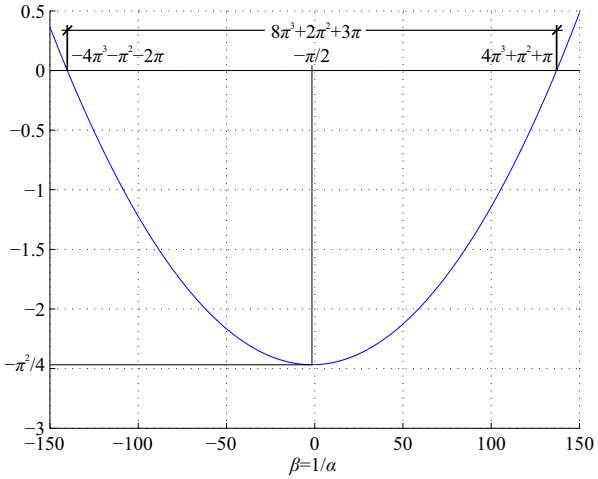

Figure 1. MLG reflectance as a function of $\beta\coloneqq 1/\alpha$.

These results are also intriguing in the context of a peculiar expression of the fine-structure constant [29] as a transcendental number

$$\alpha^{-1}=4\pi^3+\pi^2+\pi\approx 137.036303776 \tag{13}$$

 doi:10.20944/preprints202212.0045.v20

that contains a *free* π term and is very close to the physical definition (2) of α^{-1}, which according to the CODATA 2022 value is 137.035999177. We note that CODATA values are computed by averaging the measurements.

Using equations (12) and (13), we can express the negative reciprocal of the 2nd fine-structure constant α_2^{-1} that emerged in the quadratic equation (8) also as a function of π only:

$$\alpha_2^{-1} = -\pi - \alpha_1^{-1} = -4\pi^3 - \pi^2 - 2\pi \approx -140.177896429. \tag{14}$$

2.2. Transmittance and Absorptance

The transmittance (3) of MLG can also be expressed as a quadratic equation of α

$$\frac{1}{4}\mathrm{T}\pi^2\alpha^2 + \mathrm{T}\pi\alpha + (\mathrm{T}-1) = 0, \tag{15}$$

having two roots

$$\alpha = \frac{-\mathrm{T}+\sqrt{\mathrm{T}}}{\frac{1}{2}\pi\mathrm{T}} \approx (137.036)^{-1} \quad \text{and} \quad \alpha_3 = \frac{-\mathrm{T}-\sqrt{\mathrm{T}}}{\frac{1}{2}\pi\mathrm{T}} \approx (-0.7809)^{-1} \approx -1.2805, \tag{16}$$

where α_3 is the third negative fine-structure constant. Their sum hints taxicab geometry (where $\pi = 4$)

$$\alpha + \alpha_3 = -\frac{4}{\pi} \quad \forall \mathrm{T} \neq 0, \tag{17}$$

and is also independent of the value of the transmittance T. The third complementary fine-structure constant expressed by π using relations (13) and (17) is

$$\alpha_3 = -\frac{16\pi^2 + 4\pi + 5}{4\pi^3 + \pi^2 + \pi}. \tag{18}$$

Finally, the absorptance (5) of MLG can be expressed as a quadratic equation of α

$$\frac{1}{4}\mathrm{A}\pi^2\alpha^2 + (\mathrm{A}-1)\pi\alpha + \mathrm{A} = 0, \tag{19}$$

having two roots

$$\alpha = \frac{2\big((1-\mathrm{A}) - \sqrt{1-2\mathrm{A}}\big)}{\pi\mathrm{A}} \approx (137.036)^{-1} \quad \text{and} \quad \alpha_4 = \frac{2\big((1-\mathrm{A}) + \sqrt{1-2\mathrm{A}}\big)}{\pi\mathrm{A}} \approx (0.0180)^{-1} \approx 55.5387, \tag{20}$$

where α_4 is the fourth positive fine-structure constant. Their product

$$\alpha\alpha_4 = \frac{4}{\pi^2} \quad \forall \mathrm{A} \neq 0, \tag{21}$$

is also a transcendental number independent of the value of the reflectance A. The minimum of parabola (19) amounts $(2A-1)/A \approx -42.6257$ and occurs at $2(1-A)/(\pi A) \approx 27.7730$. The fourth complementary fine-structure constant expressed by π using relations (13) and (21) is

$$\alpha_4 = \frac{4}{\pi^2}\Big(4\pi^3 + \pi^2 + \pi\Big). \tag{22}$$

Preprints.org (www.preprints.org) | NOT PEER-REVIEWED | Posted: 28 August 2024 doi:10.20944/preprints202212.0045.v20

2.3. Summary

The form of the relations (13), (14) is the same (contains the same like-terms with respect to π) as the relation (126) describing the information capacity of a black body object after absorption or emission of a *particle*. Furthermore, the relation (12) corresponds to the following identity

$$\frac{\alpha + \alpha_2}{\alpha\alpha_2} = -\pi, \tag{23}$$

between the roots (10) and (11), which is also derivable from the Fresnel equations and the corresponding Euclid formula (cf. Appendix C). Because the fine-structure constants α_* are expressible by π only, we conjecture that they do not vary over time. They could not vary in the first undirected [8] and timeless [9] part of the evolution of information in the universe. Also, combining relations (23) with (17) and (21) yield

$$\frac{\alpha + \alpha_2}{\alpha\alpha_2} = \frac{\alpha + \alpha_3}{\alpha\alpha_4} = -\pi. \tag{24}$$

Furthermore, we can interpret β_* as a phase of a complex number, as shown in Figure 2. Using relations (13) and (14) along with angle sum and difference trigonometric identities we obtain

$$\begin{aligned}
z_1 &= e^{i/\alpha} = \cos(4\pi^3 + \pi^2 + \pi) + i\sin(4\pi^3 + \pi^2 + \pi) = -\cos(4\pi^3 + \pi^2) - i\sin(4\pi^3 + \pi^2) \approx 0.3682 - 0.9298i,\\
z_2 &= e^{i/\alpha_2} = \cos(-4\pi^3 - \pi^2 - 2\pi) + i\sin(-4\pi^3 - \pi^2 - 2\pi) = \cos(4\pi^3 + \pi^2) - i\sin(4\pi^3 + \pi^2) \approx -0.3682 - 0.9298i,\\
z_3 &= e^{i/\alpha_3} \approx 0.7103 - 0.7039i,\\
z_4 &= e^{i/\alpha_4} \approx 0.9998 + 0.0180i.
\end{aligned} \tag{25}$$

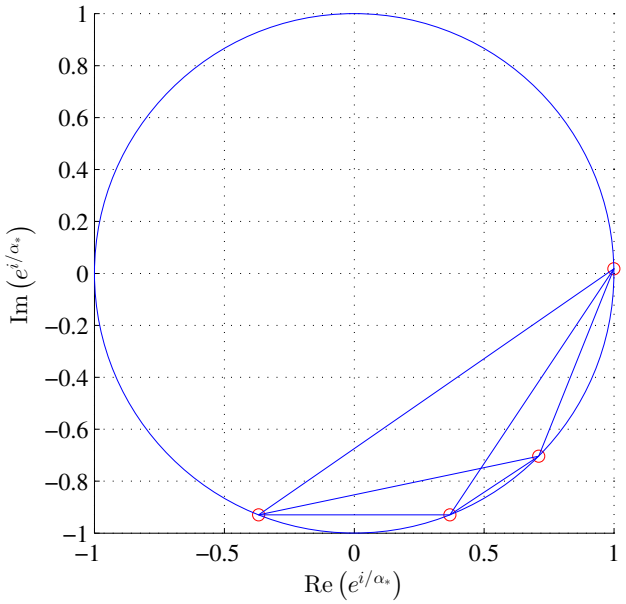

Figure 2. Four fine-structure constants as phases of a complex number $z_* := e^{i/\alpha_*}$ in order z_2, z_1, z_3, z_4 from left to right.

Finally, $\alpha_3 < \alpha_2 < 0 < \alpha < \alpha_4$. Therefore, we conclude that only α and α_2 are dual to each other and we introduce $\alpha_\star$ for α or α_2.

Using relations (13), (14), (18), and (22) the MLG coefficients (3)-(5) can be expressed simply by π (cf. Appendix A) and introduce three pairs of π-like constants for two surfaces with positive and negative Gaussian curvatures (cf. Appendix B). Interestingly, $\mathrm{T}(\alpha_4) = \mathrm{R}(\alpha)$ and $\mathrm{R}(\alpha_4) = \mathrm{T}(\alpha)$.

 doi:10.20944/preprints202212.0045.v20

In the following section, we derive the complementary sets of Planck units corresponding to the complementary fine-structure constants α_*. We shall use the subscript "$*$" as a placeholder for all four fine-structure constants, and the subscripts "$+$", "$-$" to describe respectively positive α or α_4 and negative α_2 or α_3 and quantities associated with them. Occasionally we use the subscript 1 for quantities associated with $\alpha_1 := \alpha$.

3. Complementary Sets of Planck Units

Natural units can be derived from numerous starting points [6,30] (cf. Appendices E). The central assumption in all systems of natural units is that the quotient of the unit of length ℓ_* and time t_* is a unit of speed; we call it $c = \ell_*/t_*$. It is the speed of light in vacuum c in all systems of natural units, except for Hartree and Schrödinger units, where it is $c\alpha$, and Rydberg units, where it is $c\alpha/2$. Hence, α is coupled with c in Hartree, Schrödinger, and Rydberg measurement units.

The fine-structure constant can be defined as the quotient (2) of the squared (and thus positive) elementary charge e and the squared Planck charge $\alpha = e^2/q_\mathrm{P}^2$. To accommodate the negativity of the fine-structure constants α_- discovered in the preceding section, we must introduce the imaginary Planck charge such that its square would yield a negative value.

For example, in the case of α_2

$$q_\mathrm{P}^2 = \frac{e^2}{\alpha} \quad \neq \quad q_\mathrm{P2}^2 = \frac{e^2}{\alpha_2} \quad \Rightarrow \quad q_\mathrm{P2} = \pm ae, \quad a = \frac{1}{\sqrt{\alpha_2}} \in \mathbb{I}. \tag{26}$$

Therefore

$$e^2 = q_{\mathrm{P}*}^2 \alpha_*. \tag{27}$$

We note that an imaginary $q_{\mathrm{P}-}$, which must have a physical definition analogous to q_P, requires either a real, negative speed of light or some complementary real, negative electric constant (h is positive). Let us call them c_- and $\tilde{\epsilon_0}$

$$q_\mathrm{P}^2 = 4\pi\epsilon_0\hbar c > 0, \quad q_{\mathrm{P}-}^2 = 4\pi\tilde{\epsilon_0}\hbar c_- < 0. \tag{28}$$

From this equation, we find that $\tilde{\epsilon_0} c_- < 0$, because the values of the other constants are known.

We assume the universality of the Planck constant h and the gravitational constant G. However, this assumption may be too far-reaching, given that we do not need to know the gravitational constant G or Planck constant h to find the product of the Planck length and c, $\ell_\mathrm{P} c = \sqrt{\hbar G/c}$ [31], i.e., we know how to express three physical constants $\{\hbar, G, c\}$ by two $\{\ell_\mathrm{P}, c\}$ only. This resembles a qubit, which in general requires three real numbers to be described, whereas if it encodes only one of its states, then just two real numbers suffice.

The fine-structure constant can also be defined as the ratio of Coulomb's law for two elementary charges to Newton's law of gravity for two Planck masses separated by the same *distance*. Constructing the same ratio for the remaining α_* leads to

$$\frac{1}{4\pi R^2}\frac{e^2}{\epsilon_0} = \alpha_* G \frac{m_{\mathrm{P}*}^2}{R^2}, \tag{29}$$

where the area of a 3-ball ($4\pi R^2$) in the denominator of the Coulomb force requires further investigation. Hence, the quotient of the squared Planck charge and mass must be the same for all sets of Planck units. Therefore

$$\frac{q_{\mathrm{P}*}^2}{m_{\mathrm{P}*}^2} = 4\pi\epsilon_0 G, \tag{30}$$

is independent of the unit of time (even though ϵ_0 and G are) and introduces the imaginary Planck masses $m_{\mathrm{P}-}$. The masses $m_{\mathrm{P}*}$ can be calculated from equation (30) by determining the value of the Planck charge $q_{\mathrm{P}*}$ from equation (27). From (30) we also conclude that $\tilde{\epsilon_0} = \epsilon_0 > 0$ and then by (31)

 doi:10.20944/preprints202212.0045.v20

that $\mu_2 > 0$ and $c_2 < 0$. Next, we assume that the solution of Maxwell's equations in vacuum is valid for other values of the constants involved. Let us call the unknown magnetic constant, corresponding to c_*, μ_*. Therefore,

$$\mu_0\epsilon_0c^2 = \mu_*\epsilon_0c_*^2 = 1, \tag{31}$$

from which the bivalued $c_* = \pm 1/\sqrt{\mu_*\epsilon_0}$ can be obtained. Unlike the electric constant ϵ_0, magnetic constants μ_* are independent of the unit of time. Furthermore, Maxwell's equations in vacuum are not directly dependent on the fine-structure constant(s), which is included in the magnetic constant μ_0. Finally, combining relations (27) and (28) yields

$$e^2 = 4\pi\epsilon_0\hbar c_*\alpha_*, \tag{32}$$

which establishes the universality of the elementary charge e that defines both matter and antimatter and leads to the following important relation between the speeds of light in vacuum c_*, and the fine-structure constants α_*

$$c\alpha = c_2\alpha_2 = c_3\alpha_3 = c_4\alpha_4 = \frac{e^2}{4\pi\epsilon_0\hbar}. \tag{33}$$

$c\alpha$ is also the velocity of the electron in the first circular orbit in the Bohr hydrogen atom model to which we shall return in Section 7. Because each c_* derivable from the final Maxwell equation (31) is bivalued, all sets of α_*-Planck units have four forms equal in modulus: real positive, real negative, imaginary positive and imaginary negative. However, due to the relation (33), we consider mostly real, positive α_+-Planck units and imaginary, positive α_--Planck units. We note that switching the signs of c_* in the relation (33) would require the imaginary elementary charge $e_i = ie$. Therefore, we consider real Planck units associated with the positive speed of light c_{2+} associated with α_2 in the Appendix D only.

Complementary speeds of light c_* (33) introduce complementary sets of Planck units, wherein basic α_--Planck units are imaginary since they are defined as square roots containing c_- raised to odd powers (1, 3, 5). Furthermore, the speed of electromagnetic radiation is the product of its wavelength and frequency, and these quantities would be imaginary in terms of imaginary Planck units; a negative speed of light is necessary to accommodate this.

α_2-Planck units that can be expressed, using the relation (33), in terms of base Planck units q_P, ℓ_P, m_P, t_P, and T_P are

$$q_{\mathrm{P}2} = \sqrt{4\pi\epsilon_0\hbar c_2} = q_\mathrm{P}\sqrt{\frac{\alpha}{\alpha_2}} \approx i1.8969 \times 10^{-18}\ [\mathrm{C}] \quad (|q_{\mathrm{P}2}| > |q_\mathrm{P}|), \tag{34}$$

$$\ell_{\mathrm{P}2} = \sqrt{\frac{\hbar G}{c_2^3}} = \ell_\mathrm{P}\sqrt{\frac{\alpha_2^3}{\alpha^3}} \approx i1.5622 \times 10^{-35}\ [\mathrm{m}] \quad (|\ell_{\mathrm{P}2}| < |\ell_\mathrm{P}|), \tag{35}$$

$$m_{\mathrm{P}2} = \sqrt{\frac{\hbar c_2}{G}} = m_\mathrm{P}\sqrt{\frac{\alpha}{\alpha_2}} \approx i2.2012 \times 10^{-8}\ [\mathrm{kg}] \quad (|m_{\mathrm{P}2}| > |m_\mathrm{P}|), \tag{36}$$

$$t_{\mathrm{P}2} = \sqrt{\frac{\hbar G}{c_2^5}} = t_\mathrm{P}\sqrt{\frac{\alpha_2^5}{\alpha^5}} \approx i5.0942 \times 10^{-44}\ [\mathrm{s}] \quad (|t_{\mathrm{P}2}| < |t_\mathrm{P}|), \tag{37}$$

$$T_{\mathrm{P}2} = \sqrt{\frac{\hbar c_2^5}{Gk_\mathrm{B}^2}} = T_\mathrm{P}\sqrt{\frac{\alpha^5}{\alpha_2^5}} \approx i1.4994 \times 10^{32}\ [\mathrm{K}] \quad (|T_{\mathrm{P}2}| > |T_\mathrm{P}|). \tag{38}$$

 doi:10.20944/preprints202212.0045.v20

Most Planck units derived from the α_2-Planck base units (34)-(38) are also imaginary. These include the α_2 Planck volume

$$\ell_{\mathrm{P2}}^3 = \left(\frac{\hbar G}{c_2^3}\right)^{3/2} = \ell_{\mathrm{P}}^3 \sqrt{\frac{\alpha_2^9}{\alpha^9}} \approx i3.8127 \times 10^{-105}\ [\mathrm{m}^3] \quad \left(|\ell_{\mathrm{P2}}^3| < |\ell_{\mathrm{P}}^3|\right), \tag{39}$$

the α_2 Planck momentum

$$p_{\mathrm{P2}} = m_{\mathrm{P2}} c_2 = \sqrt{\frac{\hbar c_2^3}{G}} = m_{\mathrm{P}} c \sqrt{\frac{\alpha^3}{\alpha_2^3}} \approx i6.7506\ [\mathrm{kg\ m/s}] \quad (|m_{\mathrm{P2}} c_2| > |m_{\mathrm{P}} c|), \tag{40}$$

the α_2 Planck energy

$$E_{\mathrm{P2}} = m_{\mathrm{P2}} c_2^2 = \sqrt{\frac{\hbar c_2^5}{G}} = E_{\mathrm{P}} \sqrt{\frac{\alpha^5}{\alpha_2^5}} \approx i2.0701 \times 10^9\ [\mathrm{J}] \quad (|E_{\mathrm{P2}}| > |E_{\mathrm{P}}|), \tag{41}$$

and the α_2 Planck acceleration

$$a_{\mathrm{P2}} = \frac{c_2}{t_{\mathrm{P2}}} = \sqrt{\frac{c_2^7}{\hbar G}} = a_{\mathrm{P}} \sqrt{\frac{\alpha^7}{\alpha_2^7}} \approx \pm i6.0198 \times 10^{51}\ [\mathrm{m/s^2}] \quad (|a_{\mathrm{P2}}| > |a_{\mathrm{P}}|). \tag{42}$$

However, the α_2-Planck density

$$\rho_{\mathrm{P2}} = \frac{m_{\mathrm{P2}}}{\ell_{\mathrm{P2}}^3} = \frac{c_2^5}{\hbar G^2} = \rho_{\mathrm{P}} \frac{\alpha^5}{\alpha_2^5} \approx -5.7735 \times 10^{96}\ [\mathrm{kg/m^3}] \quad (|\rho_{\mathrm{P2}}| > |\rho_{\mathrm{P}}|), \tag{43}$$

and the α_2-Planck area

$$\ell_{\mathrm{P2}}^2 = \frac{\hbar G}{c_2^3} = \ell_{\mathrm{P}}^2 \frac{\alpha_2^3}{\alpha^3} \approx -2.4406 \times 10^{-70}\ [\mathrm{m^2}] \quad \left(|\ell_{\mathrm{P2}}^2| < |\ell_{\mathrm{P}}^2|\right), \tag{44}$$

are real and negative. Interestingly, both Planck forces F_{P} and

$$F_{\mathrm{P2}} = \frac{c_2^4}{G} = \frac{c^4}{G} \frac{\alpha^4}{\alpha_2^4} = F_{\mathrm{P}} \frac{\alpha^4}{\alpha_2^4} \approx 1.3251 \times 10^{44}\ [\mathrm{N}] \quad (F_{\mathrm{P2}} > F_{\mathrm{P}}), \tag{45}$$

are strictly positive. The remaining sets of Planck units are listed in Table 1.

 doi:10.20944/preprints202212.0045.v20

Table 1. Complementary fine-structure constants α_2-α_4 and the associated physical quantities and sets of Planck units.

	α	α_2	α_3	α_4
π-form	$\frac{1}{4\pi^3+\pi^2+\pi}$	$\frac{-1}{4\pi^3+\pi^2+2\pi}$	$-\frac{16\pi^2+4\pi+5}{4\pi^3+\pi^2+\pi}$	$\frac{4}{\pi^2}(4\pi^3+\pi^2+\pi)$
α_*	0.0073	-0.0071	-1.2805	55.5387
α_*^{-1}	137.0363	-140.1779	-0.7809	0.0180
c_* [m/s]	299792458	-3.0667×10^8	-1.7084×10^6	3.9390×10^4
$q_{\mathrm{P}*}$ [C]	1.8755×10^{-18}	$1.8969 \times 10^{-18}i$	$1.4158 \times 10^{-19}i$	2.1499×10^{-20}
$\ell_{\mathrm{P}*}$ [m]	1.6162×10^{-35}	$1.5622 \times 10^{-35}i$	$3.7570 \times 10^{-32}i$	1.0731×10^{-29}
$m_{\mathrm{P}*}$ [kg]	2.1765×10^{-8}	$2.2013 \times 10^{-8}i$	$1.6430 \times 10^{-9}i$	2.4948×10^{-10}
$t_{\mathrm{P}*}$ [s]	5.3911×10^{-44}	$5.0941 \times 10^{-44}i$	$2.1991 \times 10^{-38}i$	2.7243×10^{-34}
$T_{\mathrm{P}*}$ [K]	1.4168×10^{32}	$1.4994 \times 10^{32}i$	$3.4733 \times 10^{26}i$	2.8037×10^{22}
$\ell_{\mathrm{P}*}^3$ [m^3]	4.2218×10^{-105}	$3.8124 \times 10^{-105}i$	$5.3030 \times 10^{-95}i$	1.2358×10^{-87}
$p_{\mathrm{P}*}$ [kg m/s]	6.5249	$6.7506i$	$0.0028i$	9.8272×10^{-6}
$E_{\mathrm{P}*}$ [J]	1.9561×10^9	$2.0702 \times 10^9 i$	$4.7954 \times 10^3 i$	0.3871
$a_{\mathrm{P}*}$ [m/s^2]	5.5609×10^{51}	$6.0200 \times 10^{51}i$	$7.7686 \times 10^{43}i$	1.4459×10^{38}
$\rho_{\mathrm{P}*}$ [kg/m^3]	5.1553×10^{96}	-5.7740×10^{96}	-3.0982×10^{85}	2.0188×10^{77}
$\ell_{\mathrm{P}*}^2$ [m^2]	2.6122×10^{-70}	-2.4404×10^{-70}	-1.4115×10^{-63}	1.1516×10^{-58}
$F_{\mathrm{P}*}$ [N]	1.2103×10^{44}	1.3252×10^{44}	1.2764×10^{35}	3.6072×10^{28}
μ_* [kg m C^{-2}]	1.2569×10^{-6}	1.2012×10^{-6}	0.0387	72.8061
T	$\mathrm{T}(\alpha) \approx 0.9775$	$\mathrm{T}(\alpha_2) \approx 1.0228$	$\mathrm{T}(\alpha_3) = \mathrm{T}(\alpha)$	$\mathrm{T}(\alpha_4) = \mathrm{R}(\alpha)$
A	$\mathrm{A}(\alpha) \approx 0.0224$	$\mathrm{A}(\alpha_2) \approx -0.0229$	$\mathrm{A}(\alpha_3) \approx -3.9323$	$\mathrm{A}(\alpha_4) = \mathrm{A}(\alpha)$
R	$\mathrm{R}(\alpha) \approx 1.2843 \times 10^{-4}$	$\mathrm{R}(\alpha_2) = \mathrm{R}(\alpha)$	$\mathrm{R}(\alpha_3) \approx 3.9548$	$\mathrm{R}(\alpha_4) = \mathrm{T}(\alpha)$
$\pi_1 = \pi\alpha_*/\alpha$		-3.0712	-551.2868	2.3910×10^4
$\pi_2 = \pi\alpha/\alpha_*$		-3.2136	-0.0179	4.1278×10^{-4}

Contrary to the elementary charge e (27), there is no physically meaningful *elementary mass* $M_e = \pm 1.8592 \times 10^{-9}$ [kg] satisfying the relation (36)

$$M_e^2 = \alpha_* m_{\mathrm{P}*}^2. \tag{46}$$

There is no physically meaningful *elementary length* $L_e \approx \pm 2.5927 \times 10^{-32}$ [m] satisfying the relation (35)

$$L_e^2 = \frac{\ell_{\mathrm{P}*}^2}{\alpha_*^3}, \tag{47}$$

or an *elementary temperature* $T_e \approx \pm 6.4450 \times 10^{26}$ [K] satisfying the relation (38)

$$T_e^2 = \alpha_*^5 T_{\mathrm{P}*}^2, \tag{48}$$

and close to the Hagedorn temperature of grand unified string models, or an *elementary period* $t_e = \pm 1.1851 \times 10^{-38}$ satisfying the relation (37)

$$t_e^2 = \frac{t_{\mathrm{P}*}^2}{\alpha_*^5}. \tag{49}$$

However, the relations between periods (49) and temperatures (48) are inverted. Hence, the energy-time version of Heisenberg's uncertainty principle (HUP) is saturated using energy from the equipartition theorem for one bit of information [5,6,32] both by Planck temperatures and times and *elementary* temperatures and periods (49), (48)

$$\frac{1}{2} k_{\mathrm{B}} T_{\mathrm{P}*} t_{\mathrm{P}*} = \frac{1}{2} k_{\mathrm{B}} T_e t_e = \frac{\hbar}{2}. \tag{50}$$

The Planck charge relation (27) and charge conservation principle imply that the elementary charge e, unlike mass M_e is the same in all systems of Planck units, even though the same forms of the

 doi:10.20944/preprints202212.0045.v20

relations (27) and (46) reflect the same forms of Coulomb's law and Newton's law of gravity, which are inverse-square laws.

Condensed-matter systems having two pairs of sublattices located at half-translation positions and related by multiple glide-reflection symmetries, such as palladium diselenide, make their relative quantum phases polarized into only four kinds, three of which become dark due to double destructive interference [33]. This is akin to two qubits with one fixed quantum phase. The dark quantum state does not absorb or emit photons and, therefore, is undetectable by spectroscopic means. Considering this result and the equality of the elementary charge e in all systems of Planck units that we derived based on a condensed-matter system having only one pair of sublattices, and thus analogous to only one qubit, we note the elementary charge e in these three complementary systems *defines* the dark electron of these systems. Thus $(0)000$ (blue) dark state disclosed in [33] corresponds to α-electron, $(0)0\pi\pi$ (red) state corresponds to α_2-electron, and $(0)\pi\pi0$ (green) and $(0)\pi0\pi$ (yellow) states correspond to α_3- and α_4-electrons.

In the following, where deemed appropriate, we express the physical quantities in Planck units:

$$\begin{aligned}
&M_+ \coloneqq m_+ m_{\mathrm{P}+}, && M_- \coloneqq m_- m_{\mathrm{P}-}, \quad m_+, m_- \in \mathbb{R} \\
&E_+ \coloneqq m_+ E_{\mathrm{P}+} && E_- \coloneqq m_- E_{\mathrm{P}-}, \\
&Q_+ \coloneqq qe, && Q_- \coloneqq iQ_+ = iqe, \quad q \in \mathbb{Z}, \\
&\lambda_+ \coloneqq l\ell_{\mathrm{P}}, && \lambda_- \coloneqq l_-\ell_{\mathrm{P}-}, \quad l_+ = \tfrac{2\pi}{m_+}, l_- = \tfrac{2\pi}{m_-}, \\
&\{R_+, D_+\} \coloneqq \{r_+, d_+\}\ell_{\mathrm{P}+}, && \{R_-, D_-\} \coloneqq \{r_i, d_i\}\ell_{\mathrm{P}-}, \quad r_+, d_+, r_-, d_- \in \mathbb{R},
\end{aligned} \tag{51}$$

where uppercase letters M, E, Q, λ, R, and D denote masses, energies, charges, Compton wavelengths, radii, and diameters (or *lengths*), lowercase letters m, l, etc. denote multipliers of the real α_+ and imaginary α_- Planck units, respectively, and q is an integer multiplier of the elementary charge e. The latter assumption is most likely too far-reaching, considering the fractional charges of *quasiparticles*, particularly in the open research problem of the fractional quantum Hall effect (cf. Appendix G) and energy-dependent fractional charges in electron pairing [34].

4. Black Body Objects

There are only three observable *objects* in nature that emit perfect black-body radiation: unsupported black holes (BHs, the densest), neutron stars (NSs), supported, as believed, by neutron degeneracy pressure, and white dwarfs (WDs), supported, as believed, by electron degeneracy pressure (the least dense). We collectively refer to these black-body *objects* (BBs). The spectral density in sonoluminescence, that is light emission by sound-induced collapsing gas bubbles in fluids, was also shown to have the same frequency dependence as black-body radiation [35,36]. Thus, sonoluminescence, particularly shrimpoluminescence [37], is probably emitted by collapsing micro-BBs. Micro-BH induced in glycerin by modulating acoustic waves has also been reported [38].

The term *black-body object* is not used in general relativity (GR) and standard cosmology, but standard cosmology scrunches under embarrassingly significant failings, not just *tensions* as is sometimes described, as if to somehow imply that a resolution will eventually be found [39]. In addition, James Webb Space Telescope data show multiple galaxies that grew too massive too soon after the Big Bang, which is a strong discrepancy with the Λ cold dark matter model (ΛCDM) expectations of how galaxies formed at early times at both redshifts, even when considering observational uncertainties [40]. For example, the supermassive BH of J1120+0641 quasar with mass $M_{\mathrm{BH}} = 1.52 \pm 0.17 \times 10^9 M_\odot$ assembled in less than 0.77 billion years after the Big Bang [41,42]. This is an important unresolved issue, indicating that fundamental changes to the reigning ΛCDM model of cosmology are required [40]. In particular, it is well known that entropic gravity [32] explains the galaxy rotation curves without resorting to dark matter (dark matter is not required to explain the rotation curves of certain galaxies, such as the massive relic galaxy NGC 1277 [43]), has been experimentally confirmed [44], and is decoherence-free [45].

 doi:10.20944/preprints202212.0045.v20

The term *object* as a collection of *matter* is a misnomer because it neglects the (quantum) nonlocality [9,46] that is independent of the entanglement among *particles* [47], as well as the Kochen-Specker contextuality [48], and increases as the number of *particles* increases [49,50]. Macro-realistic theories are false [51]. Thus, we use *emphasis* for (perceivably indistinguishable) *particle* and (perceivably distinguishable) *object*, as well as *matter* and *distance*. The ugly duckling theorem [52,53] asserts that every two *objects* we perceive are equally similar (or equally dissimilar). These terms do not have an absolute meaning in the ED. In particular, given the observation of *quasiparticles* in classical systems [54]. Within the ED framework, no *object* is *enclosed* in *space*. The interiors of the BBs are inaccessible to an exterior observer [55], which makes them similar to interior-less mathematical points representing real numbers on a number line. Thus, the term *object* is a particularly staring misnomer if applied to BBs.

It has been experimentally confirmed that (so-called) *accretion instability* is a fundamental physical process [56]. We conjecture that this process, which has already been recreated under laboratory conditions [57], is common for all BBs. As black-body radiation is a radiation of global thermodynamic equilibrium, it is patternless [58] (thermal noise) radiation that depends only on one parameter. In the case of BHs, this is known as Hawking [59] radiation, and this parameter is the BH temperature $T_{\mathrm{BH}} = T_{\mathrm{P}}/(2\pi d_{\mathrm{BH}})$ corresponding to the BH diameter [6] $D_{\mathrm{BH}} = d_{\mathrm{BH}}\ell_{\mathrm{P}}$. Furthermore, BHs absorb patternless information [6,60]. Therefore, because Hawking radiation depends only on the diameter of a BH, it is the same for a given BH, even though it fluctuates (cf. Section 10).

As black-body radiation is patternless, triangulated [6] BBs contain a balanced number of Planck area triangles, each having binary potential $\delta\varphi_k = -c^2 \cdot \{0,1\}$, as has been shown for BHs [6], based on the Bekenstein-Hawking (BH) entropy [55] $S_{\mathrm{BH}} = k_{\mathrm{B}}N_{\mathrm{BH}}/4$, where $N_{\mathrm{BH}} \coloneqq 4\pi R_{\mathrm{BH}}^2/\ell_{\mathrm{P}}^2 = \pi d_{\mathrm{BH}}^2$ is the information capacity of the BH surface, i.e., the $\lfloor N_{\mathrm{BH}} \rfloor \in \mathbb{N}_0$ Planck triangles corresponding to bits of information [5,6,32,55,61], and the fractional part triangle(s) having the area $\{N_{\mathrm{BH}}\}\ell_{\mathrm{P}}^2 = (N_{\mathrm{BH}} - \lfloor N_{\mathrm{BH}} \rfloor)\ell_{\mathrm{P}}^2$ too small to carry a single bit of information [5,6], where "$\lfloor x \rfloor$" is the floor function that yields the greatest integer less than or equal to its argument x.

BH entropy can be derived from the Bekenstein bound

$$S \leq \frac{2\pi k_{\mathrm{B}} RE}{\hbar c} = \pi k_{\mathrm{B}} m_1 d_1, \tag{52}$$

which defines an upper limit on the thermodynamic entropy S that can be contained within a sphere of radius R and energy E. Substituting BH (Schwarzschild) radius $R_{\mathrm{BH}} = 2GM_{\mathrm{BH}}/c^2$ and mass-energy equivalence $E_{\mathrm{BH}} = M_{\mathrm{BH}}c^2$, where M_{BH} is the BH mass, into the bound (52), it reduces to the BH entropy. In other words, the BH entropy saturates the Bekenstein bound (52). Furthermore, the Bekenstein bound can be derived from the BH entropy

$$S_{\mathrm{BH}} = \frac{1}{4}k_{\mathrm{B}}N_{\mathrm{BH}} = \frac{1}{4}k_{\mathrm{B}}\frac{4\pi R^2}{\ell_{\mathrm{P}}^2} = k_{\mathrm{B}}\frac{\pi RR}{\ell_{\mathrm{P}}^2} \leq k_{\mathrm{B}}\pi R\frac{2GE}{c^4}\frac{c^3}{\hbar G} = \frac{2\pi k_{\mathrm{B}}RE}{\hbar c}, \tag{53}$$

where we used $M \leq \frac{Rc^2}{2G}$ and $E = Mc^2$.

The patternless nature of perfect black-body radiation was derived [6] by comparing the BH entropy with the binary entropy variation $\delta S = k_{\mathrm{B}}N_1/2$ ([6] Eq. (55)), which is valid for any HS, where $N_1 \in \mathbb{N}$ denotes the number of active Planck triangles with a binary potential $\delta\varphi_k = -c^2$. Thus, the entropy of all BBs is

$$S_{\mathrm{BB}} = \frac{1}{4}k_{\mathrm{B}}N_{\mathrm{BB}}. \tag{54}$$

Furthermore, $N_1 = N_{\mathrm{BB}}/2$ confirms the patternless thermodynamic equilibrium of BBs by maximizing Shannon entropy [6]. In complex Euclidean $\mathbb{R}^a \times \mathbb{I}^b$ space, a n-ball ($n = a + bi \in \mathbb{C}$) is spherical only for $b = 0$, i.e., when perceived. Not only BBs are perfectly spherical when perceived; their mergers (cf. Section 9) are also perfectly spherical. Furthermore, the trigonometric member of its volume

 doi:10.20944/preprints202212.0045.v20

and surface formulas vanishes for the radius $r = 1/\sqrt{\pi}$ [5,17]. This is an important result since $r = 1/\sqrt{\pi}$ is a dimensionless mathematical value like π or α_*, while $R = r\ell_P = \ell_P/\sqrt{\pi}$, providing the information capacity $N = 4$ and hence one unit of BB entropy (54) is a physical one. Anyway, this corroborates the universality and applicability of BH entropy (54) to all BBs. Furthermore, some binary strings of of length $N_{BB} \geq 4$ can be assembled in less than $N_{BB} - 1$ steps. There is no disorder or uncertainty in a binary string of length $N_{BB} \leq 3$ [9].

We shall define the generalized radius of a BB (this definition applies to all HSs) having mass M_{BB} as a function of GM_{BB}/c^2 multiplier $k \in \mathbb{R}, k \geq 2$

$$R_{BB} := k\frac{GM_{BB}}{c^2}, \quad d_{BB} = 2km_{BB}, \tag{55}$$

and the generalized BB energy E_{BB} (this definition also applies to all HSs) as a function of $M_{BB}c^2$ multiplier $a \in \mathbb{R}$

$$E_{BB} := aM_{BB}c^2, \quad E_{BB} = am_{BB}E_P. \tag{56}$$

Substituting M_{BB} from the generalized radius definition (55) into the generalized BB energy definition (56) and the latter into the Bekenstein bound (52), we obtain

$$S \leq \frac{1}{2}k_B\frac{a}{k}N_{BB}, \tag{57}$$

which equals BB entropy (54) if $\frac{a}{2k} = \frac{1}{4} \Leftrightarrow a = \frac{k}{2}$. Thus, the energy (56) of all BBs with a generalized radius (55) turns into

$$E_{BB} = \frac{k}{2}M_{BB}c^2 = \frac{k}{2}m_{BB}E_P = \frac{d_{BB}}{4}E_P, \tag{58}$$

with $k = 2$ in the case of the BHs, setting the lower bound for the other BBs. We further call coefficient k the *size-to-mass ratio* (STM). This is similar to the specific volume (reciprocal of density) of BB. We derive the upper STM bound in Section 5. The energy (58) of BBs other than BHs (i.e., for $k > 2$) exceeds the mass-energy equivalence $E = Mc^2$, which is the limit of the maximum *real* energy. Therefore, we consider this surplus energy that exceeds $M_{BB}c^2$ as related to charge and we shall model it as imaginary and thus unmeasurable.

According to the no-hair theorem, all BHs general relativity (GR) solutions are characterized by only three parameters: mass, electric charge, and angular momentum. However, BHs are fundamentally uncharged, because the parameters of any conceivable BH, in particular, charged (Reissner–Nordström) and charged-rotating (Kerr–Newman) BH, can be arbitrarily altered, provided that the BH area does not decrease [62] using Penrose processes [63,64] to extract the electrostatic and/or rotational energy of BH [65]. Thus, any BH is defined by only one real parameter: its diameter, mass, temperature, energy, etc., each differing from the other by a multiplicative constant. A BH can embrace the real number that defines it as a curvature of a spherical triangle corresponding to one bit of classical information. The area of a spherical triangle is larger than that of a flat triangle defined by the same vertices and depends on its curvature.

However, it is accepted that in the case of NSs, electrons combine with protons to form neutrons, such that NSs are composed almost entirely of neutrons. However, it is never the case that all electrons and protons of an NS become neutrons. WDs are charged by definition because they are believed to be mostly composed of electron-degenerate *matter*. But how can a charged BB store both its curvature corresponding to its mass and an additional parameter corresponding to its charge? Fortunately, the relation (27) ensures that the elementary charge is the same in all systems of Planck units. Therefore, the *charge* of a spherical Planck triangle of a BB surface can link the perceivable Euclidean space $\mathbb{R}^3_\alpha \times \mathbb{I}_\alpha$ parameterized by Planck units with the parameterization provided by one of the remaining negative fine-structure constants α_-. This can be considered in a polyspherical coordinate system, in which gravitation/acceleration acts in a radial direction (with the entropic gravitation acting inwardly

 doi:10.20944/preprints202212.0045.v20

and acceleration acting in both radial directions) [6], while electrostatic acts in tangential directions. Contrary to the no-hair theorem, we characterize BBs only by mass and charge, neglecting the angular momentum because the latter introduces the notion of time, which we find redundant in the BB description of a patternless thermodynamical equilibrium. Time is required for directed exploration only [8,9].

5. Complex Energies

A complex energy formula

$$E_R := E_{M_R} + iE_{Q_R} = M_R c^2 + \frac{iQ_R}{2\sqrt{\pi\epsilon_0 G}}c^2, \tag{59}$$

where E_{M_R} and iE_{Q_R} represent the real and imaginary energies of an *object* having mass M_R and charge Q_R was proposed in ref. [66]. Equation (59) considers the real masses M_R and charges Q_R which in ref. [66] are defined in CGS units. We adopted SI units and modified this formula to a form involving real physical expressed in terms of real α_+-Planck units and imaginary quantities expressed in terms of the imaginary α_--Planck units using relations (33), (36), (41), (51), and (32) as

$$\frac{e}{2\sqrt{\pi\epsilon_0}} = \sqrt{\alpha_+ c_+ \hbar} = \sqrt{\alpha_- c_- \hbar}. \tag{60}$$

To this end, we defined the following three complex energies linking mass, imaginary mass, and charge: the complex energy of real mass and imaginary charge

$$E_{MQ_i} := E_{M_+} + E_{Q_-} = M_+ c_+^2 + \frac{Q_-}{2\sqrt{\pi\epsilon_0 G}}c_+^2 = (m_+ m_{\mathrm{P}+} + iq\sqrt{\alpha_+}m_{\mathrm{P}+})c_+^2 = (m_+ + iq\sqrt{\alpha_+})E_{\mathrm{P}+}, \tag{61}$$

of real charge and imaginary mass

$$E_{QM_i} := E_{Q_+} + E_{M_-} = \frac{Q_+}{2\sqrt{\pi\epsilon_0 G}}c_-^2 + M_- c_-^2 = (q\sqrt{\alpha_-}m_{\mathrm{P}-} + m_- m_{\mathrm{P}-})c_-^2 = \frac{\alpha_+^2}{\alpha_-^2}\left(q\sqrt{\alpha_+} + \sqrt{\frac{\alpha_+}{\alpha_-}}m_-\right)E_{\mathrm{P}+}, \tag{62}$$

and of real mass and imaginary mass

$$E_{MM_i} := M_+ c_+^2 + M_- c_-^2 = \left(m_+ + \sqrt{\frac{\alpha_+^5}{\alpha_-^5}}m_-\right)E_{\mathrm{P}+}. \tag{63}$$

We neglected the energy of real and imaginary charges E_{QQ_i}, because by equation (27), the elementary charge is the same in all systems of measurement units, and hence we use the same elementary charge multiplier q in (51). Furthermore, the mass-energy equivalence relates the mass M_+ or M_- to the speed of light c_+ or c_-, which subsequently parameterizes both parts of the energies E_{MQ_i} and E_{QM_i} (cf. Appendix F). We express all energies (61)-(63) in terms of the same Planck energy $E_{\mathrm{P}+}$ in order to be able to compare them, as we assume that they are fundamental to any *object* and *particle*. We also note that the complex conjugates E_{MQ_i} and $\overline{E_{MQ_i}}$ of the energy (61) represent respectively *particle* and *antiparticle*. We note that antimatter obeys gravity [67], which is consistent with the definition (61) and the findings of this study.

In the remainder of this section we shall analyze the energies (61)-(63) for different pairs of $\{\alpha_+, \alpha_-\}$ in order $\{\alpha_1, \alpha_2\}$, $\{\alpha_4, \alpha_2\}$, $\{\alpha_1, \alpha_3\}$, and $\{\alpha_4, \alpha_3\}$. Our aim is to determine which pair is the most plausible physically.

 doi:10.20944/preprints202212.0045.v20

Energies (61) and (62) yield two different charge energies corresponding to the elementary charge, imaginary quantum

$$E_{Q_-}(q=\pm 1)=\pm i\sqrt{\alpha_+}E_{\mathrm{P}+}\approx\pm\{1.6710\times 10^8,\ 2.8848\}i\ [\mathrm{J}], \tag{64}$$

and the - larger in modulus - real quantum

$$E_{Q_+}(q=\pm 1)=\pm\sqrt{\alpha_-}E_{\mathrm{P}-}\approx\pm\{1.7684\times 10^8,\ 5.4265\times 10^3\}\ [\mathrm{J}]. \tag{65}$$

Furthermore, $\forall q,\ \alpha_+^2 E_{Q_-}=i\alpha_-^2 E_{Q_+}$. The universal character of the charges is additionally emphasized by the real $\sqrt{\alpha}$ multiplied by i in the imaginary charge energy (61) and imaginary $\sqrt{\alpha_2}$ in the real charge energy (62).

Theorem 1. *The complex energies* (61)-(63) *cannot be all balanced complex quantities.*

Proof. The complex energies E_{MQ_i} and E_{QM_i} are balanced if their real and imaginary parts are equal in modulus. This holds for

$$q^2\alpha_+=m_+^2=-\frac{\alpha_+}{\alpha_-}m_-^2. \tag{66}$$

However, if balanced with each other, they cannot be balanced with the energy E_{MM_i}, which is balanced for

$$m_+^2=-\frac{\alpha_+^5}{\alpha_-^5}m_-^2\neq-\frac{\alpha_+}{\alpha_-}m_-^2, \tag{67}$$

defining the energy balance of uncharged masses. Similarly, the complex energies E_{QM_i} and E_{MM_i} can be balanced with each other but not with E_{MQ_i} since

$$\frac{\alpha_+^4}{\alpha_-^4}q^2\alpha_+=-\frac{\alpha_+^5}{\alpha_-^5}m_-^2=m_+^2\neq q^2\alpha_+ \tag{68}$$

and likewise for E_{MQ_i} and E_{MM_i}. □

The squared moduli of the complex energies (61)-(63), expressed in terms of the Planck energy, are

$$|E_{MQ_i}|^2=\left(M_+^2+q^2\alpha_+m_{\mathrm{P}+}^2\right)c_+^4=\left(m_+^2+q^2\alpha_+\right)E_{\mathrm{P}+}^2, \tag{69}$$

$$|E_{QM_i}|^2=\frac{\alpha_+^4}{\alpha_-^4}\left(q^2\alpha_+m_{\mathrm{P}+}^2-M_-^2\right)c_+^4=\frac{\alpha_+^4}{\alpha_-^4}\left(q^2\alpha_+-\frac{\alpha_+}{\alpha_-}m_-^2\right)E_{\mathrm{P}+}^2, \tag{70}$$

$$|E_{MM_i}|^2=\left(M_+^2-\frac{\alpha_+^4}{\alpha_-^4}M_-^2\right)c_+^4=\left(m_+^2-\frac{\alpha_+^5}{\alpha_-^5}m_-^2\right)E_{\mathrm{P}+}^2, \tag{71}$$

ad shown in Figure 3.

 doi:10.20944/preprints202212.0045.v20

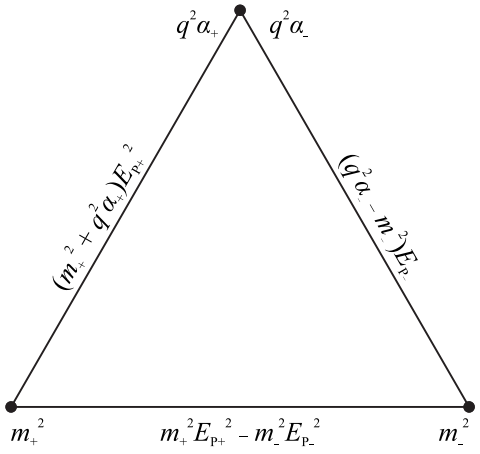

Figure 3. Squared moduli of three complex energies linking mass m_+, imaginary mass m_-, and charge q through pairs of positive and negative fine-structure constants.

Equalities of the squared moduli of the complex energies lead to the following results

$$|E_{MQ_i}|^2 = |E_{QM_i}|^2 \quad \Leftrightarrow \quad m_- = \pm\sqrt{\frac{\alpha_-}{\alpha_+}\left[q^2\alpha_+\left(1-\frac{\alpha_-^4}{\alpha_+^4}\right)-\frac{\alpha_-^4}{\alpha_+^4}m_+^2\right]}, \tag{72}$$

$$|E_{MQ_i}|^2 = |E_{MM_i}|^2 \quad \Leftrightarrow \quad m_- = \pm q\sqrt{-\frac{\alpha_-^5}{\alpha_+^4}} = \pm q\{0.0807, 1.3935\times10^{-9}, 3.4846\times10^{4}, 6.0157\times10^{-4}\}, \tag{73}$$

$$|E_{QM_i}|^2 = |E_{MM_i}|^2 \quad \Leftrightarrow \quad m_+ = \pm q\sqrt{\frac{\alpha_+^5}{\alpha_-^4}} = \pm q\{0.0894, 4.5170\times10^{8}, 2.7741\times10^{-6}, 1.4019\times10^{4}\}, \tag{74}$$

Because the mass multiplier $m_- \in \mathbb{R}$, the square root argument must be nonnegative in equation (72), which leads to (the sign of this inequality changes, as $\alpha_- < 0$)

$$m_+ \geq |q|\sqrt{\alpha_+\left(\frac{\alpha_+^4}{\alpha_-^4}-1\right)} \approx |q|\{0.0263, 4.5170\times10^{8}, 0.0854i, 1.4019\times10^{4}\}, \tag{75}$$

which is imaginary for $\sqrt{\alpha(\alpha^4/\alpha_3^4-1)}$ ruling out the third pair of alphas $\{\alpha_1, \alpha_3\}$. Otherwise, we would have to exclude *objects* having the same energies E_{MQ_i} and E_{QM_i} from our model. Furthermore, for $q = 0$ equation (72) yields

$$m_- = \pm m_+\sqrt{-\frac{\alpha_-^5}{\alpha_+^5}} \approx \pm m_+\left\{0.9449, 1.8699\times10^{-10}, 4.0791\times10^{5}, 8.0722\times10^{-5}\right\}, \tag{76}$$

which corresponds to equation (67).

Furthermore, the relation (75) means that the masses of the uncharged micro-BHs ($q = 0$) can be arbitrary ($m \geq 0$). However, micro NSs and micro WDs, which are also in thermodynamic equilibrium, are charged. Thus, even a single elementary charge ($q = 1$) of a white dwarf renders its minimum allowable mass (75) $M_{\mathrm{WD}} \geq 5.7275\times10^{-10}$ [kg] comparable to the mass of a sand grain.

 doi:10.20944/preprints202212.0045.v20

Theorem 2. *Moduli of the complex energies* (69)-(71) *are equal*

$$|E_{MQ_i}|^2 = |E_{QM_i}|^2 = |E_{MM_i}|^2 = \left(1+\frac{\alpha_2^4}{\alpha^4}\right)m^2E_P^2 = \left(1+\frac{\alpha^4}{\alpha_2^4}\right)q^2\alpha E_P^2 = -\left(1+\frac{\alpha_2^4}{\alpha^4}\right)\frac{\alpha^9}{\alpha_2^9}m_i^2E_P^2 := A^2E_P^2, \quad A\in\mathbb{R}, \tag{77}$$

for

$$q^2\alpha = -\frac{\alpha^5}{\alpha_2^5}m_i^2 = \frac{\alpha_2^4}{\alpha^4}m^2, \quad m_i^2 = -\frac{\alpha_2^9}{\alpha^9}m^2 \approx 0.8155m^2. \tag{78}$$

Proof. If the squared moduli (69)-(71) are equal to some constant energy then $q^2\alpha$ drops out by subtracting $|E_{MQ_i}|^2 - \frac{\alpha_2^4}{\alpha^4}|E_{QM_i}|^2$, yielding

$$m^2 + \frac{\alpha}{\alpha_2}m_i^2 = A^2\left(1-\frac{\alpha_2^4}{\alpha^4}\right). \tag{79}$$

Subtracting this from $|E_{MM_i}|^2$ yields

$$m_i^2 = -A^2\frac{\alpha_2^9}{\alpha^5(\alpha^4+\alpha_2^4)}, \tag{80}$$

which substituted into the relation (79) yields

$$m^2 = A^2\frac{\alpha^4}{\alpha^4+\alpha_2^4}. \tag{81}$$

Finally, substituting m^2 (81) into equation $|E_{MQ_i}|^2$ (69) yields

$$q^2\alpha = A^2\frac{\alpha_2^4}{\alpha^4+\alpha_2^4}. \tag{82}$$

□

We can interpret the squared generalized energy of the BBs (58) as the squared modulus of each of the complex energies (69)-(71). That is, for E_{MQ_i} (61) and for E_{MM_i} (63), we assume that the real mass energy $E_{\mathrm{BB}} = M_{\mathrm{BB}}c^2$ of the BB is the observable real part of this complex energy. For $|E_{MQ_i}|^2$ (69) we have

$$\frac{k^2}{4}m_{\mathrm{BB}}^2 = m_{\mathrm{BB}}^2 + q_{\mathrm{BB}}^2\alpha_+ \quad \Leftrightarrow \quad q_{\mathrm{BB}}\sqrt{\alpha_+} = \pm m_{\mathrm{BB}}\sqrt{\frac{k^2}{4}-1}, \tag{83}$$

where $q_{\mathrm{BB}}^2\alpha_+$ represents the charge surplus energy exceeding $M_{\mathrm{BB}}c^2$. We note that $k=2$ implies $q_{\mathrm{BB}}=0$, confirming the vanishing charge of BHs. For $|E_{MM_i}|^2$ (71) we have

$$\frac{k^2}{4}m_{\mathrm{BB}}^2 = m_{\mathrm{BB}}^2 - \frac{\alpha_+^5}{\alpha_-^5}m_{i\mathrm{BB}}^2 \quad \Leftrightarrow \quad m_{i\mathrm{BB}} = \pm m_{\mathrm{BB}}\sqrt{\frac{\alpha_-^5}{\alpha_+^5}\left(1-\frac{k^2}{4}\right)}, \tag{84}$$

where the square root argument must be nonnegative, which implies (along with (83)), as expected, $k\geq 2$, where $k=2$ implies $m_{i\mathrm{BB}}=0$. Finally, for $|E_{QM_i}|^2$ (70) we have

$$\frac{k^2}{4}m_{\mathrm{BB}}^2 = \frac{\alpha_+^4}{\alpha_-^4}\left(q_{\mathrm{BB}}^2\alpha_+ - \frac{\alpha_+}{\alpha_-}m_{i\mathrm{BB}}^2\right) \quad \Leftrightarrow \quad m_{i\mathrm{BB}} = \pm m_{\mathrm{BB}}\sqrt{\frac{\alpha_-}{\alpha_+}\left[\frac{k^2}{4}\left(1-\frac{\alpha_-^4}{\alpha_+^4}\right)-1\right]}, \tag{85}$$

 doi:10.20944/preprints202212.0045.v20

where we substituted $q_{\mathrm{BB}}^2\alpha_+$ as a function of m_{BB}^2 from equation (83). Comparison of $m_{i\mathrm{BB}}$ given by (85) with m_i given by (72) also leads to $k \geq 2$, and for $k = 2$ or $q = 0$ corresponds to the balance of uncharged masses (67), (76) which are unrelated to any assumptions regarding BB energy and independent of STM. Comparing equations (72), as a function of charge q, and (85), as a function of the STM k, leads, as expected, to the relation (83).

Furthermore, the square root argument in equation (85) must be nonnegative, because $m_{\mathrm{BB}}, m_{i\mathrm{BB}} \in \mathbb{R}$. This leads to the maximum STM-bound

$$k \leq \frac{2}{\sqrt{1-\frac{\alpha_-^4}{\alpha_+^4}}} = k_{\max} \approx \{\underline{6.7933}, 2.0000, 6.4949 \times 10^{-5} i, 2.0000\}, \tag{86}$$

where again third pair of examined alphas $\{\alpha_1, \alpha_3\}$ must be ruled out, while pairs $\{\alpha_2, \alpha_4\}$ and $\{\alpha_3, \alpha_4\}$ do not allow to extend our model above the STM of BH. The relations (83) and (85) are shown in Figure 4 for α and α_2.

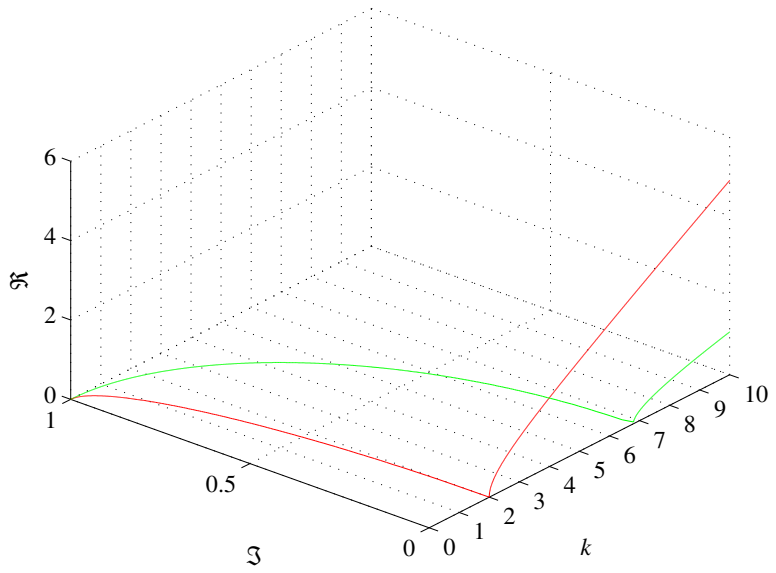

Figure 4. Ratios of imaginary mass $M_{i\mathrm{BB}}$ to real mass M_{BB} (green) and real charge $q_{\mathrm{BB}} m_{\mathrm{P}} \sqrt{\alpha}$ to M_{BB} (red) of a BB as a function of the size-to-mass ratio $0 \leq k \leq 10$ for $\{\alpha, \alpha_2\}$. The mass $M_{i\mathrm{BB}}$ is imaginary for $k \lessapprox 6.79$. The charge q_{BB} is real for $k \geq 2$.

The maximum STM-bound $k_{\max}$ (86) sets the bounds on BB energy (58), mass, and radius (55)

$$R_{\mathrm{BH}} = \frac{2GM_{\mathrm{BB}}}{c^2} \leq R_{\mathrm{BB}} \leq \frac{k_{\max} GM_{\mathrm{BB}}}{c^2}. \tag{87}$$

In particular, using the relations (51), $2m_{\mathrm{BB}} \leq r_{\mathrm{BB}} \leq k_{\max} m_{\mathrm{BB}}$ or $r_{\mathrm{BB}}/k_{\max} \leq m_{\mathrm{BB}} \leq r_{\mathrm{BB}}/2$.

From the relation (78) we see that uncharged BHs ($q = 0$) cannot remain in a nonvanishing equilibrium of complex energies (77), even though they are in thermodynamic equilibrium. It was shown [5] based on the Mandelstam-Tamm [68], Margolus–Levitin [69], and Levitin-Toffoli [70] theorems on the quantum orthogonalization interval that a BH is represented by a qubit $|\psi_{\mathrm{BH}} = \frac{1}{\sqrt{2}}(|0 + |E_{\mathrm{BH}})$ in an equal superposition of the eigenstates corresponding to the BH energy $E_{\mathrm{BH}} = M_{\mathrm{BH}}c^2$ and vanishing ground state energy. However, such a nonvanishing equilibrium of complex

 doi:10.20944/preprints202212.0045.v20

energies (77) is possible for charged BBs. We obtain it by substituting squared generalized energy of the BBs (58) into equation (77) as $A^2 = \frac{1}{4}k^2 m_{\mathrm{BB}}^2$ and solving for $\left(1+\alpha_-^4/\alpha_+^4\right)m_{\mathrm{BB}}^2$. This yields

$$k_{\mathrm{eq}} = 2\sqrt{1+\frac{\alpha_-^4}{\alpha_+^4}} \approx \{\underline{2.7665}, 2.0000, 6.1586\times 10^4, 2.0000\} \tag{88}$$

where all three energies are equal. The equilibrium k_{eq} (88) and maximum k_{max} (86) STMa satisfy $k_{\mathrm{eq}}^2 + 16/k_{\mathrm{max}}^2 = 8$ (which resolves to $2 \leq |k_{\mathrm{eq}}| < 2\sqrt{2}, |k_{\mathrm{max}}| \geq \sqrt{2}, \forall k_{\mathrm{eq}}, k_{\mathrm{max}} \neq 0 \in \mathbb{R}$).

The relations (75), (86), and (88) show that the negative fine-structure constant α_- corresponding to α is α_2 not α_3. As we have seen in Section 2.3, α and α_2 are dual to each other. The BB having the STM $k_{\mathrm{eq}} \approx 2.7665$ (88) and the elementary charge ($q^2 = 1$) would have mass $M_{\mathrm{BB}}(k_{\mathrm{eq}}) \approx \pm 1.9455\times 10^{-9}$ [kg], imaginary mass $M_{i\mathrm{BB}}(k_{\mathrm{eq}}) \approx \pm i 1.7768\times 10^{-9}$ [kg], corresponding to the Compton wavelength $\lambda_{\mathrm{BB}}(k_{\mathrm{eq}}) \approx \pm 1.1361\times 10^{-33}$ [m], and the imaginary Compton wavelength $\lambda_{i\mathrm{BB}}(k_{\mathrm{eq}}) \approx \pm i 1.2160\times 10^{-33}$ [m]. On the other hand, equation (83) provides the BB charge in equilibrium (77) as $q_{\mathrm{BB}}(k_{\mathrm{eq}}) \approx 11.1874\, m_{\mathrm{BB}}$ and the limit of the BB charge $q_{\mathrm{BB}}(k_{\mathrm{max}}) \approx 37.9995\, m_{\mathrm{BB}}$.

We note that BBs with STMs $2 \leq k \leq 3$ are referred to as *ultracompact* [71], where $k_{\mathrm{ps}} = 3$ is a photon sphere radius, at which, according to an accepted photon sphere definition, the strength of gravity *forces photons to travel in orbits*. The author wonders why the photons would not *travel in orbits* at a radius $R = GM/c^2$ corresponding to the *orbital* velocity $v_{\mathrm{orb}}^2 = GM/R$ of mass M. Obviously, according to the ED principle, photons do not *travel*. Any *object* that undergoes complete gravitational collapse passes through an ultracompact stage [72], where $k < 3$. Collapse can be approached by gradual accretion, increasing the mass to the maximum stable value, or by the loss of angular momentum [72]. During the loss of angular momentum, the star passes through a sequence of increasingly compact configurations until it finally collapses and becomes a BH. It was also pointed out [73] that for a neutron star of constant density, the pressure at the center would become infinite if $k = 2.25$, which is the radius of the maximal sustainable density for gravitating spherical *matter* given by Buchdahl's theorem. It was shown [74] that this limit applies to any well-behaved spherical star, where the density increases monotonically with the radius. Furthermore, some observers would measure a locally negative energy density if $k < 2.6(6)$ thus breaking the dominant energy condition, although this may be allowed [75]. As the surface gravity increases, photons from further behind the NS become visible. At $k \approx 3.52$ the entire NS surface becomes visible [76]. The relative increase in brightness between the maximum and minimum of a light curve is greater for $k < 3$ than for $k > 3$ [76]. Furthermore, $k_{\mathrm{c}} = \sqrt{27} \approx 5.1962$ defining a photon capture radius [77], the effective radius for capturing photons that approach the black hole from infinity is about 76% of k_{max} (86). Therefore, the equilibrium and maximum STM ratios (88), (86) satisfying $k_{\mathrm{eq}} < k_{\mathrm{ps}} < k_{\mathrm{c}} < k_{\mathrm{max}}$ are well within the range of radii of ultracompact *objects* researched in the state-of-the-art within the GR framework.

However, aside from the Schwarzschild radius, derivable from the escape velocity $v_{esc}^2 = 2GM/R$ of mass M by setting $v_{esc}^2 = c^2$, and discovered in 1783 by John Michell [78], all the remaining significant radii of GR are only approximations. GR neglects the value of the Planck constant and the fine-structure constants α and α_2, which, similar to π or the base of the natural logarithm, are fundamental constants of nature. Constructive criticism of GR can be found, for example, in [79–85].

Therefore, we conjecture that k_{eq} is the correct value of the photon sphere radius and k_{max} is the correct value of a photon capture radius. These radii are indirectly measured by the Event Horizon Telescope (EHT), a telescope array consisting of a global network of radio telescopes, each associated with an atomic clock. The signals collected by each telescope are stored along with time stamps and subsequently shipped to one location to be synchronized and processed. The EHT observational targets are the Milky Way's BH, Sagittarius A* (Sgr A*) and the M87* BH at the center of the Messier 87 galaxy. The EHT data processing model assumes a Kerr BH (uncharged, spinning) [77,86] and is suitable for prograde accretion disks [86] (spinning in the same direction as a BH). The first assumption

 doi:10.20944/preprints202212.0045.v20

is congruent with our results; in this and in the preceding sections we have shown that BHs are fundamentally uncharged.

The processed Sgr A* and M87* signals revealed ring-like structures surrounding these BHs, which were compared with a large suite of general-relativistic magnetohydrodynamics (GRMHD) simulations [77,86]. However, the GRMHD simulations turned out to be more variable than the observed signals and only a few configurations could satisfy the full set of observational constraints apart from variability, hinting that more work is needed to fully explore the physical parameter space and to understand this variability, as these variations challenge standard approaches to interferometric analysis. Subsequently, measurements of the first in an infinite series of photon rings around M87* were reported [87] based on simultaneous modeling and imaging of the EHT signals. However, the photon ring calculated by this method turned out to be much brighter than expected, while it should be emitting only around 20 percent of the light in the image, as general relativity predicts [88]. Therefore, it may be just picking out an unrelated structure in the image [89] and M87* and Sgr A* EHT observations have yet to experimentally resolve any photon ring [90–93]. This ambiguity requires further research of these ring-like structures revealed by the EHT within the ED framework, considering the equilibrium and maximum STM ratios $k_{\rm eq}$ (88) and $k_{\rm max}$ (86) that may accurately describe them.

6. Complex Forces

The complex energies (61)-(63) define the complex forces (similarly to the complex energy of real masses and charges (59); cf. ref. [66] Eq. (7)). Using the relations (51), we obtain the following three complex products of energies

$$E_{12mq_i} \coloneqq E_{1MQ_i}E_{2MQ_i}/E_{\rm P}^2 = m_1m_2 - q_1q_2\alpha + i\sqrt{\alpha}(m_1q_2 + m_2q_1), \tag{89}$$

$$E_{12qm_i} \coloneqq E_{1QM_i}E_{2QM_i}/E_{\rm P}^2 = \frac{\alpha^4}{\alpha_2^4}\left(\alpha q_1q_2 + \frac{\alpha}{\alpha_2}m_{i1}m_{i2} + \sqrt{\frac{\alpha}{\alpha_2}}\sqrt{\alpha}(m_{i1}q_2 + m_{i2}q_1)\right), \tag{90}$$

$$E_{12mm_i} \coloneqq E_{1MM_i}E_{2MM_i}/E_{\rm P}^2 = m_1m_2 + \frac{\alpha^5}{\alpha_2^5}m_{i1}m_{i2} + \sqrt{\frac{\alpha^5}{\alpha_2^5}}(m_1m_{i2} + m_2m_{i1}), \tag{91}$$

where E_{1AB_i} is the energy of object 1 and E_{2AB_i} is the energy of object 2. Their squared moduli are

$$\begin{aligned}
|E_{12mq_i}|^2 &= m_1^2m_2^2 + \alpha^2q_1^2q_2^2 + \alpha\left(m_1^2q_2^2 + m_2^2q_1^2\right),\\
|E_{12qm_i}|^2 &= \frac{\alpha_+^{10}}{\alpha_-^{10}}\left(m_{i1}^2m_{i2}^2 + \alpha_2^2q_1^2q_2^2 - \alpha_2\left(m_{i1}^2q_2^2 + m_{i2}^2q_2^2\right)\right),\\
|E_{12mm_i}|^2 &= m_1^2m_2^2 + \frac{\alpha^{10}}{\alpha_2^{10}}m_{i1}^2m_{i2}^2 - \frac{\alpha^5}{\alpha_2^5}(m_1^2m_{i2}^2 + m_2^2m_{i1}^2).
\end{aligned} \tag{92}$$

Products of energies (89)-(91) define three complex forces acting over a real *distance* R_+

$$F_{AB_i} = \frac{G}{c^4R_+^2}E_{1AB_i}E_{2AB_i} = \frac{F_{\rm P}}{r_+^2}E_{12ab_i}, \tag{93}$$

and three complex forces acting over an imaginary *distance* R_-

$$\tilde{F}_{AB_i} = \frac{G}{c_2^4R_-^2}E_{1AB_i}E_{2AB_i} = \frac{\alpha_2}{\alpha}\frac{F_{\rm P}}{r_-^2}E_{12ab_i}, \tag{94}$$

where $A, B \in \{M, Q\}$ and $a, b \in \{m, q\}$. We express the forces (93) and (94) in terms of the Planck force $F_{\rm P}$ in order to compare them, which yields

$$\alpha_2r_+^2F_{AB_i} = \alpha r_-^2\tilde{F}_{AB_i}. \tag{95}$$

 doi:10.20944/preprints202212.0045.v20

In the case of two charged masses m_1 and m_2 in a balanced state, such as a nucleus and an electron cloud of an atom in its non-ionized state, $q_1 = -q_2$ and switching the signs of charges ($q_1 \to -q_2$, $q_2 \to -q_1$) provides complex conjugates of the energies (89) and (90), which - after such switch - represent antimatter.

7. Extended Bohr Model

The Bohr model of the hydrogen atom is based on three assumptions that can be conveniently expressed in terms of Planck units using relations (51). The first assumption of a natural number of electron wavelengths λ_e that fits along the circumference of the electron's orbit of radius R becomes:

$$n\lambda_e = 2\pi R \quad \Leftrightarrow \quad nl_e = 2\pi r, \quad n \in \mathbb{N}. \tag{96}$$

The second assumption, de Broglie's relation between electron mass M_e, velocity V_e and wavelength becomes

$$\lambda_e = \frac{h}{M_e V_e} = \frac{2\pi\hbar}{M_e V_e} \quad \Leftrightarrow \quad l_e = \frac{2\pi}{m_e v_e}, \; V_e := v_e c, \; v_e \in \mathbb{R}. \tag{97}$$

Finally, the third assumption postulated equality between the centripetal force exerted on the electron *orbiting around* the proton (assuming an infinite mass of the latter) and the Coulomb force between the electron and proton becomes:

$$\frac{M_e V_e^2}{R} = \frac{1}{4\pi\epsilon_0}\frac{e^2}{R^2} \quad \Leftrightarrow \quad m_e v_e^2 r = \frac{e^2}{4\pi\epsilon_0\hbar c} = \alpha. \tag{98}$$

It is remarkable that such a simple postulate alone, expressed in terms of Planck units, introduces the fine-structure constant α. Joining relations (96) and (97) yields

$$m_e v_e r = n, \tag{99}$$

which combined with (98) and using the relation (33) yields

$$V_e = v_e c = \frac{1}{n}\alpha c \quad \Leftrightarrow \quad v_e = \frac{1}{n}\alpha, \tag{100}$$

Thus, in the first circular orbit ($n = 1$) of this model, the electron velocity factor $v_e = \alpha$. In the Bohr model of atoms other than hydrogen this equality of forces is *extended* to a point-like set of Z electrons orbiting around a nucleus, where Z is the atomic number.

Furthermore, since the proton and the electron have different signs of the elementary charge e, the Coulomb force should be considered negative in this model.

To quantify charges, we assume that the centripetal force acting on the electron is equal to the complex force F_{MQ_i} (93) with the product of real mass and imaginary charge energies (89) and, motivated by the short multiplication formula $(a+b)(a-b)$ and the two-body problem we describe, use the reduced mass of the proton-electron system. This yields

$$\frac{m_e m_p}{m_e + m_p}\frac{v_e^2}{r} = \frac{m_e m_p + \alpha + i\sqrt{\alpha}(m_e - m_p)}{r^2}, \tag{101}$$

where we set $q_e = -1$ and $q_p = 1$ as the electron and proton charges, respectively, $m_e, m_p \in \mathbb{R}$ from the electron mass $M_e = m_e m_{\mathrm{P}} = 9.1094 \times 10^{-31}$ [kg] and the proton mass $M_p = m_p m_{\mathrm{P}} = 1.6726 \times 10^{-27}$ [kg]. The equation (101) yields complex velocity

$$v_e = \sqrt{\frac{m_e + m_p}{r}\left(1 + \frac{\alpha}{m_e m_p}\right) + i\frac{\sqrt{\alpha}}{r}\frac{m_e^2 - m_p^2}{m_e m_p}} \approx 7.2993 \times 10^{-3} - i3.2816 \times 10^{-21} \approx \alpha \tag{102}$$

 doi:10.20944/preprints202212.0045.v20

assuming that R is equal to the Bohr radius $a_0 = 5.2918 \times 10^{-11}$ [m] or the complex radius

$$R = \left(\frac{m_e + m_p}{v_e^2} \left(1 + \frac{\alpha}{m_e m_p} \right) + i \frac{\sqrt{\alpha}}{v_e^2} \frac{m_e^2 - m_p^2}{m_e m_p} \right) \ell_{\mathrm{P}} \approx (5.2946 \times 10^{-11} - i4.7607 \times 10^{-29}) \text{ [m]} \approx a_0 \tag{103}$$

assuming that the Bohr model gives the velocity of the electron, that is, $v_e = \alpha$. However, neglecting their insignificant imaginary parts, they correspond to their Bohr model counterparts. This is because the gravitational attraction between the proton and the electron in hydrogen atom (10^{-47} N) is negligible compared to the Coulomb force between them (10^{-8} N).

We further note that switching the signs of charges ($q_e = 1, q_p = -1$) provides complex conjugates of the relation (101), which in this case describes the antihydrogen. Thus, we conjecture that the energy generated by a hydrogen-antihydrogen collision, predicted by this extended Bohr model, is

$$E_{\mathrm{H}MQ_i} + E_{\bar{\mathrm{H}}MQ_i} = 2(m_e m_p + \alpha) E_{\mathrm{P}} \approx 2.8549 \times 10^7 \text{[J]}. \tag{104}$$

Expressed in terms of Planck units and the reduced mass of the proton-electron system, the Rydberg constant for hydrogen is

$$R_{\mathrm{H}} = \frac{m_e m_p}{m_e + m_p} \frac{\alpha_*^2}{4\pi \ell_{\mathrm{P}}} \approx 1.0968 \times 10^7 \text{ [1/m]}, \tag{105}$$

The inverse of the corresponding Rydberg formula for hydrogen can be expressed using the relation (13) for α as

$$\frac{m_e m_p}{m_e + m_p} l = \frac{4\pi}{\alpha^2} \frac{n_1^2 n_2^2}{n_2^2 - n_1^2} = \frac{n_1^2 n_2^2}{n_2^2 - n_1^2} 4\pi^3 (16\pi^4 + 8\pi^3 + 9\pi^2 + 2\pi + 1), \tag{106}$$

using the wavelength relation (51) and α expression (13). The coefficients $\{16, 8, 9, 2, 1\}$ form part of the OEIS sequence A158565 for $n = 10$.

8. BB Complex Gravity and Temperature

We can use the complex force F_{MQ_i} (93) with the product (89) (i.e., complex Newton's law of universal gravitation) to calculate the BB surface gravity g_{BB}, assuming an uncharged ($q_2 = 0$) test mass m_2 and comparing this force with Newton's 2nd law of motion

$$\frac{F_{\mathrm{P}}}{r_{\mathrm{BB}}^2} (m_{\mathrm{BB}} m_2 + i\sqrt{\alpha_+} m_2 q_{\mathrm{BB}}) = M_2 g_{\mathrm{BB}} = m_2 m_{\mathrm{P}} \hat{g}_{\mathrm{BB}} a_{\mathrm{P}}, \quad \hat{g}_{\mathrm{BB}} = \frac{1}{r_{\mathrm{BB}}^2} (m_{\mathrm{BB}} + i\sqrt{\alpha_+} q_{\mathrm{BB}}), \tag{107}$$

where $g_{\mathrm{BB}} = \hat{g}_{\mathrm{BB}} a_{\mathrm{P}}$, $\hat{g}_{\mathrm{BB}} \in \mathbb{R}$. Substituting $q_{\mathrm{BB}}\sqrt{\alpha_+}$ from the BB energy relation (83) and the mass taken from the generalized BB radius (55) $r_{\mathrm{BB}} = k m_{\mathrm{BB}}$ into the relation (107) yields

$$\hat{g}_{\mathrm{BB}} = \frac{1}{k r_{\mathrm{BB}}} \left(1 \pm i \sqrt{\frac{k^2}{4} - 1} \right), \tag{108}$$

which reduces to BH surface gravity for $k = 2$ and in modulus

$$\hat{g}_{\mathrm{BB}}^2 = \frac{1}{k^2 r_{\mathrm{BB}}^2} \left(1 + i\sqrt{\frac{k^2}{4} - 1} \right) \left(1 - i\sqrt{\frac{k^2}{4} - 1} \right) = \frac{1}{4 r_{\mathrm{BB}}^2}. \tag{109}$$

for all k and is remarkably independent of α_*. In particular,

$$g_{\mathrm{BB}}(k_{\max}) = \pm \frac{a_{\mathrm{P}}}{d_{\mathrm{BB}}} (0.2944 \pm 0.9557i), \tag{110}$$

 doi:10.20944/preprints202212.0045.v20

$$g_{\mathrm{BB}}(k_{\mathrm{eq}}) = \pm\frac{a_{\mathrm{P}}}{d_{\mathrm{BB}}}(0.7229 \pm 0.6909i). \tag{111}$$

The BB surface gravity (108) leads to the generalized complex Hawking blackbody radiation equation:

$$T_{\mathrm{BB}} = \frac{\hbar}{2\pi c k_{\mathrm{B}}} g_{\mathrm{BB}} = \frac{T_{\mathrm{P}}}{k\pi d_{\mathrm{BB}}}\left(1 \pm i\sqrt{\frac{k^2}{4} - 1}\right), \tag{112}$$

describing the BB temperature by including its charge in the imaginary part, which also for $k = 2$ and in modulus reduces to the BH temperature for all k. In a commonly used, equivalent form it is

$$T_{\mathrm{BB}} = \frac{\hbar c^3}{2k^2\pi G M_{\mathrm{BB}} k_{\mathrm{B}}}\left(1 \pm i\sqrt{\frac{k^2}{4} - 1}\right). \tag{113}$$

In particular,

$$T_{\mathrm{BB}}(k_{\mathrm{max}}) = \frac{T_{\mathrm{P}}}{2\pi d_{\mathrm{BB}}}\left(\frac{\sqrt{\alpha_+^4 - \alpha_-^4}}{\alpha_+^2} \pm i\frac{\alpha_-^2}{\alpha_+^2}\right) \tag{114}$$

$$T_{\mathrm{BB}}(k_{\mathrm{eq}}) = \frac{T_{\mathrm{P}}}{2\pi d_{\mathrm{BB}}}\frac{\alpha_+^2 \pm i\alpha_-^2}{\sqrt{\alpha_+^4 + \alpha_-^4}} \tag{115}$$

reduce to the BH temperature for $\alpha_- = 0$. Therefore, a universe without the negative fine structure constants α_- (i.e., with $\alpha_- = 0$) would be a black hole disallowing the directed exploration [8,9] of the evolution of information [1–4,6,7]. This kind of exploration requires imaginary time [6]. And we cannot zero α_2 as we would have to neglect the *existence* of graphene, estimated to form about 1.9% of total interstellar carbon [94] and recently discovered on the Moon [95].

9. BB Mergers

As the entropy (Boltzmann, Gibbs, Shannon, von Neumann) of independent systems is additive, a merger of BB_1 and BB_2 having entropies (54) $S_1 = \frac{1}{4}k_{\mathrm{B}}\pi d_1^2$ and $S_2 = \frac{1}{4}k_{\mathrm{B}}N_2$, produces a BB_C with entropy (we drop the HS subscripts in this section for clarity)

$$S_1 + S_2 = S_C \quad \Leftrightarrow \quad d_1^2 + d_2^2 = d_C^2, \tag{116}$$

which shows that the resultant information capacity is the sum of the information capacities of the merging components. Thus, a merger of two primordial BHs, each with the Planck length diameter, the reduced Planck temperature $\frac{T_{\mathrm{P}}}{2\pi}$ (the largest physically significant temperature [5]) produces a BH having $d_{\mathrm{BH}} = \pm\sqrt{2}$ which represents the minimum BH diameter allowing for the notion of time [5]. In comparison, a collision of the latter two BHs produces a BH with $d_{\mathrm{BH}} = \pm 2$ and the triangulation defining only one precise diameter between its poles (cf. [6] Figure 3(b)), which is also recovered from HUP (cf. Appendix E).

Substituting the generalized diameter (55) into the entropy relation (116) establishes a Pythagorean relation between the generalized energies (58) of the merging components and the merger

$$\frac{k_C^2}{4}m_C^2 = \frac{k_1^2}{4}m_1^2 + \frac{k_2^2}{4}m_2^2, \quad \forall m_j \in \{\mathbb{R}, \mathbb{I}\}. \tag{117}$$

It is accepted that gravitational events observations alone allow measuring the masses of the merging components, setting a lower limit on their compactness, but it does not exclude mergers that are more compact than neutron stars, such as *quark stars*, BHs, or more exotic *objects* [96]. We note in passing that describing the registered gravitational events as *waves* is misleading: normal modulation

 doi:10.20944/preprints202212.0045.v20

of the gravitational potential, registered by LIGO and Virgo interferometers, and caused by rotating (in the merger case, inspiral) *objects* is wrongly interpreted as a gravitational wave understood as a carrier of gravity [97]. It has also been shown that from a mathematical point of view, the quadrupolar waves in a quantum spin nematic are in one-to-one correspondence with quantized gravitational waves in a flat, 4-dimensional spacetime [98].

The accepted value of the Chandrasekhar WD mass limit, which prevents its collapse into a denser form, is $M_{\rm Ch} \approx 1.4\ M_\odot$ [99] and the accepted value of the analogous Tolman-Oppenheimer-Volkoff NS mass limit is $M_{\rm TOV} \approx 2.9\ M_\odot$ [100,101]. There is no accepted value for the BH mass limit. The conjectured value is $5 \times 10^{10}\ M_\odot \approx 9.95 \times 10^{40}$ kg. We note in passing that a BH with a surface gravity equal to the Earth's surface gravity (9.81 m/s^2) would require a diameter of $D_{BH} \approx 9.16 \times 10^{15}$ m (slightly less than one light year) [6] and mass $M_{BH} \approx 3.08 \times 10^{42}$ kg exceeding the conjectured limit. The masses of most registered merging components go well beyond $M_{\rm TOV}$. From those that do not, most of the total or final masses exceed this limit. Therefore, these mergers (BH $\leftrightarrows$ BH, BH $\leftrightarrows$ NS, BH $\leftrightarrows$ WD, NS $\leftrightarrows$ NS, NS $\leftrightarrows$ WD, WD $\leftrightarrows$ WD) are classified as BH mergers. Only a few were classified otherwise, including GW170817, GW190425, GW200105, and GW200115, as listed in Table 2.

Table 2. Selected BB mergers discovered with LIGO and Virgo. Masses in $M_\odot$.

Event	M_1	M_2	M_C	k_1	k_2	k_C
GW170817	$1.46^{+0.12}_{-0.10}$	$1.27^{+0.09}_{-0.09}$	2.8	4.39	4.39	3.03
GW190425	$2.00^{+0.6}_{-0.2}$	$1.4^{+0.3}_{-0.3}$	$3.4^{+0.3}_{-0.1}$	4.39	4.39	3.15
GW200105	$8.9^{+1.2}_{-1.5}$	$1.9^{+0.3}_{-0.2}$	$10.9^{+1.1}_{-1.2}$	2.76	4.39	2.38
GW200115	$5.7^{+1.8}_{-2.1}$	$1.5^{+0.7}_{-0.3}$	$7.1^{+1.5}_{-1.4}$	3	4.39	2.64

Equation (117) explains the measurements of large masses of BB mergers with at least one charged merging component without resorting to any hypothetical types of exotic stellar *objects* such as *quark stars*. Interferometric data, available online at the Gravitational Wave Open Science Center (GWOSC) portal[1], indicates that the total mass of a merger is the sum of the masses of the merging components. Thus

$$m_C = m_1 + m_2 \quad \Leftrightarrow \quad m_C^2 = m_1^2 + m_2^2 + 2m_1m_2 \quad \Leftrightarrow \quad \begin{cases} m_C^2 \geq m_1^2 + m_2^2 & \text{if} \quad m_1m_2 \geq 0 \\ m_C^2 \leq m_1^2 + m_2^2 & \text{if} \quad m_1m_2 \leq 0 \end{cases}. \tag{118}$$

We can use the squared moduli $|E_{MQ_i}|^2$, $|E_{QM_i}|^2$, and $|E_{MM_i}|^2$ (83)-(84) and the relation (117) to derive some information about the merger from equation (117). We shall initially assume $m_j \geq 0 \Rightarrow m_1m_2 \geq 0$, since negative masses, similar to negative lengths, and their products with positive ones, are (in general [102]) inaccessible for direct observation, unlike charges. $|E_{MQ_i}|^2$ (83) with the first inequality (118) yields:

$$|E_{MQ_i}|_C^2 = |E_{MQ_i}|_1^2 + |E_{MQ_i}|_2^2, \quad m_C^2 = m_1^2 + m_2^2 + (q_1^2 + q_2^2)\alpha - q_C^2\alpha \geq m_1^2 + m_2^2, \quad q_C^2 \leq q_1^2 + q_2^2, \tag{119}$$

On the other hand, $|E_{QM_i}|^2$ (85) with inequality (119) leads to ($\alpha_- < 0$, and thus the direction of the inequality is reversed):

$$q_C^2 \leq q_1^2 + q_2^2 \quad \Rightarrow \quad m_{iC}^2 \geq m_{i1}^2 + m_{i2}^2. \tag{120}$$

But $|E_{MM_i}|^2$ (84) with the first inequality (118) leads to:

$$m_C^2 \geq m_1^2 + m_2^2 \quad \Rightarrow \quad m_{iC}^2 \leq m_{i1}^2 + m_{i2}^2, \tag{121}$$

[1] https://www.gw-openscience.org/eventapi/html/allevents

 doi:10.20944/preprints202212.0045.v20

contradicting inequality (120) ($\alpha_{-}^{5} < 0$), while $|E_{MM_i}|^2$ with inequality (120) leads to:

$$m_{iC}^2 \geq m_{i1}^2 + m_{i2}^2 \quad \Rightarrow \quad m_C^2 \leq m_1^2 + m_2^2, \tag{122}$$

contradicting the first inequality (118) and is consistent with the second inequality (118) introducing the product of positive and negative masses. $|E_{QM_i}|^2$ with inequality (121) yields:

$$m_{iC}^2 \leq m_{i1}^2 + m_{i2}^2 \quad \Rightarrow \quad q_C^2 \geq q_1^2 + q_2^2, \tag{123}$$

contradicting the inequality (120) and so on.

The additivity of the entropy (116) of statistically independent merging BBs, both in global thermodynamic equilibrium, defined by their generalized radii (55), introduces the energy relation (117). This relation, universality of the charges (27), and the BB complex energies (69)-(71) establish imaginary, negative, and mixed masses during the merger. The BB merger spreads as a gravitational event associated with a fast radio burst (FRB) event, as reported [103] based on the gravitational event GW1904251 and FRB 20190425A event[2]. Furthermore, IXPE[3] observations show that the polarized X-rays detected from 4U 0142+61 pulsar exhibit a 90° linear polarization swing from low to high photon energies [104]. In addition, direct evidence for a magnetic field strength reversal based on the observed sign change and extreme variation of FRB 20190520B's rotation measure, which changed from $\sim$ 10000 $[\text{rad} \cdot \text{m}^{-2}]$ to $\sim$ -16000 $[\text{rad} \cdot \text{m}^{-2}]$ between June 2021 and January 2022, has been reported [105], and such extreme rotation measure reversal has never been observed before in any FRB or any astronomical object. It has been suggested that outside the GR, merging BHs may differ from their GR counterparts [106]. Furthermore, it was experimentally confirmed [107], based on the registered gravitational event GW170817, that BB mergers are perfectly spherical. It is concluded [107] that an additional process seems necessary to make the merger distribution uniform. However, one can hardly expect the collision of two perfectly spherical, patternless thermal noises to produce an aspherical pattern instead of another perfectly spherical patternless noise. Where would information about this pattern come from at the moment of collision? From the point of impact? No point of impact can be considered unique on the patternless surface.

During the merger, the STM ratio k_C decreases, making the BB_C denser until it becomes a BH for $k_C = 2$ and no further charge reduction is possible (see Figure 4). From equation (117) and the first inequality (118), we see that this holds for

$$k_C^2 \left(m_1^2 + m_2^2 \right) \leq k_1^2 m_1^2 + k_2^2 m_2^2. \tag{124}$$

For two merging BHs $k_1 = k_2 = 2$ and the relation (124) yields $k_C^2 \leq 4 \Rightarrow k_C = 2 = k_{\text{BH}_C}$. On the other hand, if $m_1 = m_2$ then $k_C \leq \sqrt{(k_1^2 + k_2^2)/2}$. The tendency to decrease the STM, given by relation (124), is reflected in the merger statistics registered by LIGO and Virgo interferometers: the registered fraction of BH mergers is much higher than might be expected by chance.

Table 2 lists the STM ratios k_{BB_C} calculated according to equation (117), which provide the measured mass M_{BB_C} of the merger and satisfy inequality (124). The STM ratios k_{BB_1} and k_{BB_2} of the merging components were arbitrarily selected based on their masses, considering the limit of mass M_{TOV} of the NS.

---

[2] Data available online at the Canadian Hydrogen Intensity Mapping Experiment (CHIME) portal (https://www.chime-frb.ca/catalog).

[3] X-ray Polarimetry Explorer (https://ixpe.msfc.nasa.gov).

 doi:10.20944/preprints202212.0045.v20

10. BB Fluctuations

A relation [108] (p.160) describing a BH information capacity, having an initial information capacity[4] $N_j = 4\pi R_j^2/\ell_{\rm P}^2$, after absorption of a *particle* having the Compton wavelength equal to the BH radius R_j

$$N_{j+1}^{A} = 64\pi^3 \frac{\ell_{\rm P}^2}{R_j^2} + 32\pi^2 + 4\pi \frac{R_j^2}{\ell_{\rm P}^2}, \tag{125}$$

was subsequently generalized [6] (Eq. (18)) to all Compton wavelengths $\lambda = l\ell_{\rm P} = \frac{2\pi}{m}\ell_{\rm P}$ (or frequencies $\nu = c/\lambda = 1/(lt_{\rm P})$) and thus to all radiated Compton energies $E = mE_{\rm P}$, $m \in \mathbb{R}$ absorbed $(+)$ or emitted $(-)$ by a BH as

$$N_{j+1}^{A/E}(m) = 64\pi^3 \frac{1}{l^2} \pm 16\pi^2 \frac{d}{l} + \pi d^2 = 16\pi m^2 \pm 8\pi dm + \pi d^2. \tag{126}$$

Equation (126) can be further generalized, using the generalized diameter $d = 2k\hat{m}$ (55), to all BBs as follows

$$\Delta N^{A/E} := N_{j+1}^{A/E}(k, m) - N_j = 16\pi m(m \pm k\hat{m}), \tag{127}$$

where $\hat{m}$ represents the BB mass, and its roots are

$$m^{A/E} = \{0, \mp k\hat{m}\} = \left\{0, \mp \frac{d}{2}\right\} = \{0, \mp r\}, \tag{128}$$

where it vanishes. Thus, in general, BB changes its information capacity by:

$$\Delta N^{A} \begin{cases} > 0 & m \in (-\infty, -k\hat{m}) \cap (0, \infty) \\ = 0 & m = \{-k\hat{m}, 0\} \\ < 0 & m \in (-k\hat{m}, 0) \end{cases}, \quad \Delta N^{E} \begin{cases} > 0 & m \in (-\infty, 0) \cap (k\hat{m}, \infty) \\ = 0 & m = \{0, k\hat{m}\} \\ < 0 & m \in (0, k\hat{m}) \end{cases}, \tag{129}$$

absorbing or emitting energy m with $\min(\Delta N) = -4\pi k^2\hat{m}^2$ at $m = \pm k\hat{m}/2$, as shown in Figure 5. Equation (129) shows that, depending on its mass $\hat{m}$, a BB can expand or contract by emitting or absorbing energy m [6]. However, expansion by emission ($\Delta N^E > 0$), for example, requires energy $m > k\hat{m}$ exceeding the mass-energy equivalence of BB for $k > 2$, which is consistent with the results presented in Section 5. We note that the same form of the relation (127), expressed as

$$N_{j+1}^{A/E}(\hat{m}, l) = 64\pi^3 \frac{1}{l^2} \pm 32\pi^2 \frac{k\hat{m}}{l} + 4\pi k^2\hat{m}^2 \tag{130}$$

contains the same like terms with respect to π as the transcendental expressions for the fine-structure constants (13) and (14), which requires further investigation. The forms of the fine-structure constants (18) and (22) are different.

---

[4] We drop the HS subscripts in this section for clarity.

 doi:10.20944/preprints202212.0045.v20

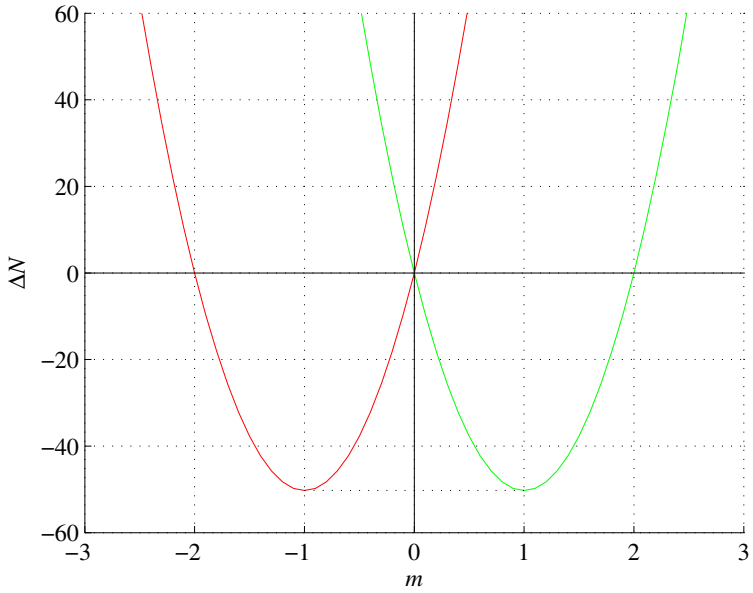

Figure 5. BB information capacity variations ΔN after absorption (red) or emission (green) of energy m ($k = 2$, $\hat{m} = 1$).

11. Discussion

Complex, imaginary, and negative physical quantities are the subject of research. In particular, the subject of scientific research is the thermodynamics in the complex plane. For example, Lee–Yang zeros [109,110] and photon-photon thermodynamic processes under negative optical temperature conditions [111] have been experimentally observed. Furthermore, the rendering of synthetic dimensions through space modulations has recently been suggested because it does not require any active materials or other external mechanisms to break time-reversal symmetry [112]. Complexified geodesics are investigated [113] and it was shown that from a geometric point of view the unitary symmetries U(1) and SU(2) stem fundamentally from Schwarzschild and Reissner-Nordström metrics through spacetime complexification if a new Euclidean metric on a complex Hermitian manifold is provided [114]. In Lorentz signature, a Hermitian structure must necessarily be complex-valued, so its integrability properties are more subtle than in the Euclidean case [115].

Physical quantities accessible for direct everyday observation are mostly real and positive with the negativity of *distances*, velocities, accelerations, etc., induced by the assumed orientation of *space*. Quantum measurement results, for example, are the necessarily *real* eigenvalues of Hermitian operators. Unlike charges, negative, real masses are also generally inaccessible for direct observations. However, dissipative coupling between excitons and photons in an optical microcavity leads to the formation of exciton polaritons with negative masses [102]. In Section 9, we show that negative masses also result from the merging of BBs.

The notion of atemporality, related to the prebiotic, timeless [9] part of the evolution of information in the universe, was also investigated [116] on a black hole (BH) surface as the dynamical mechanism responsible for the transition from a regime with a real-valued interval to an imaginary interval via the Wick rotation. The Wick rotation between real and imaginary intervals was also analyzed in the context of kinematics on holographic spheres [6] and quantum orthogonalization intervals of BHs [5].

By Noether's theorem, the conservation of energy (7) between three Fresnel coefficients for the normal incidence of electromagnetic radiation on monolayer graphene is associated with a symmetry between the fine-structure constant α and π. This symmetry establishes three complementary fine-structure constants, of which two are negative, wherein all fine-structure constants are related to each other through the constant of π, which indicates that they do not vary over time. The complementary fine-structure constants are associated with their own sets of Planck units that allow for

 doi:10.20944/preprints202212.0045.v20

different parameterization of the perceivable space $\mathbb{R}^3_\alpha \times \mathbb{I}_\alpha$ Euclidean space parameterized by the fine-structure constant α. Since the elementary charge and the products $c_*\alpha_*$ are the same in all these four parameterizations, the complementary electrons correspond to dark states recently discovered in condensed-matter systems having two pairs of sublattices.

As the two sets of basic Planck units are real and two are imaginary, we have applied four complex pairs of masses and charges defined by $\{\alpha_+, \alpha_-\}$ to the complex energy formula [66] defining three complex energies (61) and (62). The generalized energy (58) of all perfect black-body *objects* (black holes, neutron stars, and white dwarfs) with a generalized radius $R_{\rm BB} = kR_{\rm BH}/2$, where $R_{\rm BH}$ is the Schwarzschild radius, exceeds the mass-energy equivalence if $k > 2$. However, the complex energies (61)-(63) allow storage of this excess energy in their imaginary parts. Further analysis of this model showed that the negative complementary fine-structure constant established by the graphene reflectance is dual to the fine-structure constant and Appendix D presents some arguments to support the claim that α parameterization sets favorable conditions for biological evolution to emerge. The lower bound on the mass of a charged black-body *object* is $M_{\rm BB} > 5.7275 \times 10^{-10}$ [kg] and the upper bound on a white dwarf radius is $R_{\rm WD} \lesssim 3.3967\ R_{\rm BH}$, where $R_{\rm BH}$ is the Schwarzschild radius of the white dwarf mass. A charged black-body *object* is in the equilibrium of complex energies if its radius $R_{\rm eq} \approx 1.3833\ R_{\rm BH}$, which is close to the photon sphere radius $R_{\rm ps} = 1.5\ R_{\rm BH}$, and is marginally greater than the locally negative energy density bound of $4/3\ R_{\rm BH}$. The maximum radius of the black-body *object* is $R_{\rm max} \approx 3.3967\ R_{\rm BH}$, which is close to the photon capture radius $R_{\rm c} = \sqrt{27}\ R_{\rm BH}/2 \approx 2.5981\ R_{\rm BH}$. The complex force between real masses and imaginary charges leads to the complex black-body object's surface gravity and generalized Hawking radiation complex temperature. Furthermore, on the basis of the Bohr model for the hydrogen atom, we show that complex conjugates of this force represent atoms and antiatoms. The proposed model considers the value(s) of the fine-structure constant(s), which is(are) otherwise neglected in general relativity, and explains the registered (GWOSC) high masses of neutron star mergers and the associated fast radio bursts (CHIME) without resorting to any hypothetical types of exotic stellar *objects*.

MLG is a truly 2-dimensional material with no thickness. Although its thickness is reported [117] as 0.37 [nm] with other reported values up to 1.7 [nm], these results are not credible, considering that 0.335 [nm] is the established interlayer *distance* and consequently the thickness of bilayer graphene: the thickness of bilayer graphene is not $2 \times 0.37 + 0.335 = 1.075$ [nm]. In the context of the results of this study, graphene is a *keyhole* to ED. The history of graphene is also instructive. Discovered in 1947 [118], graphene was long considered an *academic material* until it was eventually pulled from graphite in 2004 [119] using ordinary Scotch tape (introduced into the market in 1932). These fifty-seven years, along with twenty-nine years (1935-1964) between the condemnation of quantum theory as *incomplete* [120] and Bell's mathematical theorem [121] asserting that it is not true, and the fifty-eight years (1964-2022) between the formulation of this theorem and the 2022 Nobel Prize in Physics for its experimental *loophole-free* confirmation, should remind us that Max Planck, the genius who discovered Planck units, has also discovered Planck's principle.

Acknowledgments: The author truly thanks his wife, Magdalena Bartocha, for her support since this research [122,123] began; Wawrzyniec Bieniawski for inspiring discussions, constructive ideas concerning the layout of this paper, and his feedback concerning the sections on BB mergers and BB fluctuations; Piotr Masierak for constructive and insightful remarks; Mariola Bala for handling these esoteric vapors under control; and Andrzej Tomski for defining the scalar product for the real/imaginary Euclidean spaces $\mathbb{R}^a \times \mathbb{I}^b$ (1).

Abbreviations

 doi:10.20944/preprints202212.0045.v20

The following abbreviations are used in this paper:

ED	emergent dimensionality
EMR	electromagnetic radiation
MLG	monolayer graphene
T	transmittance
R	reflectance
A	absorptance
α_*	any of the fine-structure constants
$\alpha_\star$	α or α_2
α_+	α or α_4
α_-	α_2 or α_3
BH	black hole
NS	neutron star
WD	white dwarf
BB	black-body object
HS	holographic sphere
STM	size-to-mass ratio
GR	general relativity
HUP	Heisenberg's uncertainty principle

Appendix A. Mlg Transmittance, Absorptance, and Reflectance as Functions of π Only

With definitions of α (13), α_2 (14), α_3 (18), and (22) MLG Fresnel coefficients (3), (4), and (5) can be expressed simply by π. For $\alpha^{-1} = 4\pi^3 + \pi^2 + \pi$ (13) and for α_4 (22) they are

$$\mathrm{T}(\alpha) = \mathrm{R}(\alpha_4) = \frac{4\left(4\pi^2+\pi+1\right)^2}{\left(8\pi^2+2\pi+3\right)^2} \approx 0.9775, \tag{A1}$$

$$\mathrm{A}(\alpha) = \mathrm{A}(\alpha_4) = \frac{4\left(4\pi^2+\pi+1\right)}{\left(8\pi^2+2\pi+3\right)^2} \approx 0.0224, \tag{A2}$$

$$\mathrm{R}(\alpha) = \mathrm{T}(\alpha_4) = \frac{1}{\left(8\pi^2+2\pi+3\right)^2} \approx 1.2843 \times 10^{-4}. \tag{A3}$$

For $\alpha_2^{-1} = -4\pi^3 - \pi^2 - 2\pi$ (14) they are

$$\mathrm{T}(\alpha_2) = \frac{4\left(4\pi^2+\pi+2\right)^2}{\left(8\pi^2+2\pi+3\right)^2} \approx 1.0228, \tag{A4}$$

$$\mathrm{A}(\alpha_2) = -\frac{4\left(4\pi^2+\pi+2\right)}{\left(8\pi^2+2\pi+3\right)^2} \approx -0.0229, \tag{A5}$$

with $\mathrm{R}(\alpha_2) = \mathrm{R}(\alpha)$ and for α_3 (18) they are

$$\mathrm{A}(\alpha_3) = \frac{48\pi^2+12\pi+16}{(8\pi^2+2\pi+3)^2} - 4 \approx -3.9323, \tag{A6}$$

$$\mathrm{R}(\alpha_3) = \frac{(16\pi^2+4\pi+5)^2}{(8\pi^2+2\pi+3)^2} \approx 3.9548, \tag{A7}$$

with $\mathrm{T}(\alpha_3) = \mathrm{T}(\alpha)$. $\mathrm{A}(\alpha) > 0$ and $\mathrm{A}(\alpha_2) < 0$ imply a *sink* and *source*, respectively, whereas the opposite holds for T, as illustrated schematically in Figure A1. We conjecture that the negative A and T values exceeding 100% for α_2 (11) and (14) could be explained in terms of graphene spontaneous EMR emission.

 doi:10.20944/preprints202212.0045.v20

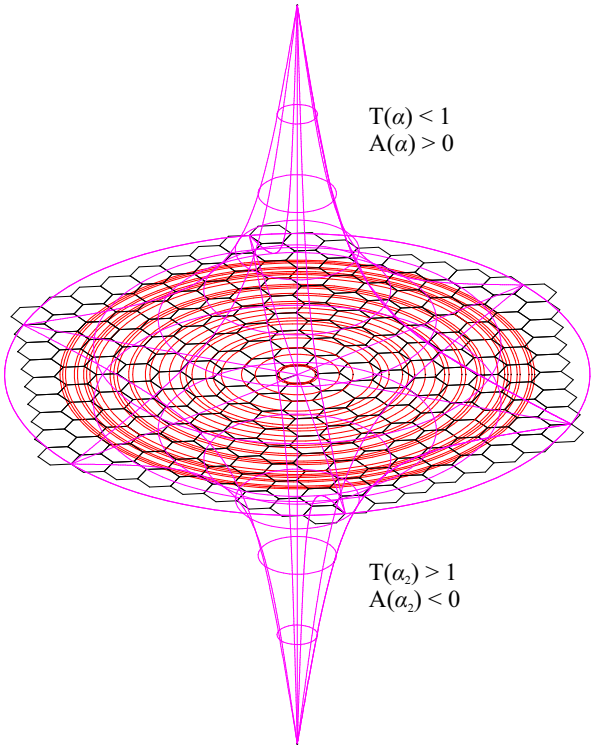

Figure A1. Illustration of the concepts of negative absorptance and excessive transmittance of EMR under normal incidence on MLG for $\{\alpha, \alpha_2\}$.

Appendix B. π-like Constants

The quadratic equation (8) can also be solved for π, which yields two roots.

$$\pi(\mathrm{R}, \alpha_\star)_1 = \frac{2\sqrt{\mathrm{R}}}{\alpha_\star(1-\sqrt{\mathrm{R}})} \quad \text{and} \quad \pi(\mathrm{R}, \alpha_\star)_2 = \frac{-2\sqrt{\mathrm{R}}}{\alpha_\star(1+\sqrt{\mathrm{R}})}, \tag{A8}$$

dependent on R and $\alpha_\star$, where $\alpha_\star$ indicates α or α_2. This can be further evaluated using the MLG reflectance R (4) or (A3), yielding four, yet only three, distinct possibilities,

$$\pi_1 = \pi(\alpha)_1 = -\pi\frac{4\pi^2+\pi+1}{4\pi^2+\pi+2} = \pi\frac{\alpha_2}{\alpha} \approx -3.0712, \tag{A9}$$

$$\pi(\alpha)_2 = \pi(\alpha_2)_1 = \pi \approx 3.1416, \quad \text{and} \tag{A10}$$

$$\pi_2 = \pi(\alpha_2)_2 = -\pi\frac{4\pi^2+\pi+2}{4\pi^2+\pi+1} = \pi\frac{\alpha}{\alpha_2} \approx -3.2136. \tag{A11}$$

The modulus of π_1 (A9) corresponds to a convex surface with a positive Gaussian curvature, whereas the modulus of π_2 (A11) corresponds to a negative Gaussian curvature. The product $\pi_1\pi_2 = \pi^2$ is independent of $\alpha_\star$, the quotient $\pi_1/\pi_2 = \alpha_2^2/\alpha^2$ is not directly dependent on π, and $|\pi_1 - \pi| \neq |\pi - \pi_2|$. It remains to be determined whether each of these π-like constants describes the ratio of the circumference of a circle drawn on the respective surface to its diameter (π_c) or the ratio of the area of this circle to the square of its radius (π_a). These definitions produce different results for curved surfaces, whereas $\pi_a > \pi_c$ on convex surfaces and $\pi_a < \pi_c$ on saddle surfaces [124]. The remaining π-like constants corresponding to α_3 and α_4 are listed in Table 1.

 doi:10.20944/preprints202212.0045.v20

Appendix C. Mlg Fresnel Equation and Euclid's Formula

The Fresnel equation for the normal incidence of EMR at the boundary of two media with refractive indices n_1 and n_2 is

$$\mathrm{R_F} + \mathrm{T_F} = \frac{(n_1 - n_2)^2}{(n_1 + n_2)^2} + \frac{(2\sqrt{n_1 n_2})^2}{(n_1 + n_2)^2} = 1. \tag{A12}$$

Substituting MLG reflectance (4) and the sum of transmittance (3) and absorptance (5) into the Fresnel equation (A12) yields

$$\frac{(n_1 - n_2)^2}{(n_1 + n_2)^2} = \frac{\frac{1}{4}\pi^2\alpha^2}{\left(1 + \frac{\pi\alpha}{2}\right)^2}, \quad \frac{4n_1 n_2}{(n_1 + n_2)^2} = \frac{1 + \pi\alpha}{\left(1 + \frac{\pi\alpha}{2}\right)^2}, \tag{A13}$$

which resolves to $n_1 = 1$ independent on α and two roots for n_2

$$n_2(\alpha) = \left\{1 + \pi\alpha, \frac{1}{1 + \pi\alpha}\right\} = \{1.0229, 0.9776\}, \tag{A14}$$

satisfying

$$1 + \pi\alpha = \frac{1}{1 + \pi\alpha_2}, \tag{A15}$$

which corresponds to the identity (23). The refractive index $n_2 \approx 1.0229$ is close to that of liquid helium $n \approx 1.025$ at 3 K. The refractive index $n_2 \approx 0.9776$ is close to the refractive index of water $n = 0.99999974 = 1 - 2.6 \times 10^{-7}$ for X-ray radiation at a photon wavelength of 0.04 nm. We note that these results are different from the complex refractive index of MLG ($\tilde{n}_g = 2.4 - 1.0i$ at 532 nm to $\tilde{n}_g = 3.0 - 1.4i$ at 633 nm at room temperature). However, because $n_1 = 1$, the equation (A14) relates to the absolute ($n = c/V$) refractive indices; it models MLG as a boundary between vacuum and some other bulk medium. Refractive indices (A14) correspond to the phase velocities

$$V\left(-\frac{\alpha_2}{\alpha}\right) = -c\frac{\alpha}{\alpha_2} = -c_2, \quad V\left(-\frac{\alpha}{\alpha_2}\right) = -c\frac{\alpha_2}{\alpha} = -\frac{c^2}{c_2} \approx 2.9307 \times 10^8 \text{ [m/s]} \tag{A16}$$

using the relation (33). We note that the phase velocity of light $-c_2 > c$ does not carry information and thus can be faster than the speed of light in vacuum c.

On the other hand, the Fresnel equation (A12) has the same form as the Euclid's formula for generating Pythagorean triples $a = k^2 - l^2$, $b = 2kl$, $c = k^2 + l^2$

$$\frac{(k^2 - l^2)^2}{(k^2 + l^2)^2} + \frac{(2kl)^2}{(k^2 + l^2)^2} = 1, \tag{A17}$$

with $k^2 = n_1$ and $l^2 = n_2$. Substituting MLG reflectance (4) and the sum of transmittance (3) and absorptance (5) into the Euclid formula (A17) yields

$$\begin{aligned} k &= \left\{\sqrt{\pi\alpha + 1}, -\sqrt{\pi\alpha + 1}, \sqrt{\frac{1}{\pi\alpha + 1}}, -\sqrt{\frac{1}{\pi\alpha + 1}}\right\} \approx \{\pm 1.0114, \pm 0.9887\}, \\ l &= \{1, 1, 1, 1\}, \end{aligned} \tag{A18}$$

 doi:10.20944/preprints202212.0045.v20

generating four right triangles with edges

$$\begin{aligned} a(\alpha) &= \left\{ \pi\alpha, \pi\alpha, \frac{-\pi\alpha}{\pi\alpha+1}, \frac{-\pi\alpha}{\pi\alpha+1} \right\} \approx \{0.0229x2, -0.0224x2\}, \\ b(\alpha) &= \left\{ 2\sqrt{\pi\alpha+1}, -2\sqrt{\pi\alpha+1}, \frac{2}{\sqrt{\pi\alpha+1}}, \frac{-2}{\sqrt{\pi\alpha+1}} \right\} \approx \{\pm 2.0228, \pm 1.9775\}, \\ c(\alpha) &= \left\{ \pi\alpha+2, \pi\alpha+2, \frac{\pi\alpha+2}{\pi\alpha+1}, \frac{\pi\alpha+2}{\pi\alpha+1} \right\} \approx \{2.0229x2, 1.9776x2\}, \end{aligned} \tag{A19}$$

and

$$\begin{aligned} a(\alpha_2) &\approx \{-0.0224x2, 0.0229x2\}, \\ b(\alpha_2) &\approx \{\pm 1.9775, \pm 2.0228\}, \\ c(\alpha_2) &\approx \{1.9776x2, 2.0229x2\}. \end{aligned} \tag{A20}$$

In each case, different edge lengths satisfy $\pi\alpha = -\pi\alpha_2/(\pi\alpha_2+1)$, which also corresponds to the identity (23). Furthermore

$$c(\alpha_\star) - a(\alpha_\star) = 2, \quad b(\alpha_\star)^2 = 4\sqrt{a(\alpha_\star)+1}. \tag{A21}$$

We further note that $a(\alpha_\star) \approx -\mathrm{A}(\alpha_\star)$, (A2), (A5) and $|b(\alpha_\star)| \approx \mathrm{T}(\alpha_\star)+1$, (A1), (A4).

Appendix D. Why α Is Better for Biological Evolution than α_2?

The probability that two nuclear *particles* a and b will undergo nuclear fusion by overcoming their electrostatic barriers is given by Gamow–Sommerfeld factor

$$p(E) = e^{-\sqrt{\frac{E_\mathrm{G}}{E}}}, \tag{A22}$$

where

$$E_\mathrm{G} := 2\frac{m_a m_b}{m_a+m_b} E_\mathrm{P} (\pi\alpha Z_a Z_b)^2 \tag{A23}$$

is the Gamow energy, m_a, m_b are the masses of those *particles* in terms of α or α_2 Planck units (51) and Z_a, Z_b are their respective atomic numbers.

As $(\pi\alpha)^2 \approx 5.2557 \times 10^{-4}$ is larger than $(\pi\alpha_2)^2 \approx 5.0227 \times 10^{-4}$, the probability (A22) is higher for the same dimensionless parameters m_*, Z_*. Therefore, perceivable $(\mathbb{R}^3_\alpha \times \mathbb{I}_\alpha)$-space provides more favorable conditions for the evolution of information (by nuclear fusion) than nonperceivable $(\mathbb{R}^3_{c_{2+}} \times \mathbb{I}_{c_{2+}})$-space parameterized with negative α_2, positive c_{2+} and with imaginary charge due to the relation (33).

Furthermore, the c_{2+}-Planck energy $E_{\mathrm{P}2+}$ and temperature $T_{\mathrm{P}2+}$ are higher than the Planck energy E_P and temperature T_P. Therefore, the perceivable $(\mathbb{R}^3_\alpha \times \mathbb{I}_\alpha)$-space provides more favorable conditions for the evolution of information than would be provided by nonperceivable $(\mathbb{R}^3_{c_{2+}} \times \mathbb{I}_{c_{2+}})$-space, also owing to the minimum energy principle.

Appendix E. Planck Units and HUP

Perhaps the simplest derivation of the squared Planck length is based on HUP

$$\delta P_\mathrm{HUP} \delta R_\mathrm{HUP} \geq \frac{\hbar}{2} \quad \text{or} \quad \delta E_\mathrm{HUP} \delta t_\mathrm{HUP} \geq \frac{\hbar}{2}, \tag{A24}$$

where δP_HUP, δR_HUP, δE_HUP, and δt_HUP denote momentum, position, energy, and time uncertainties, respectively. Replacing energy uncertainty $\delta E_\mathrm{HUP} = \delta M_\mathrm{HUP} c^2$ with mass uncertainty using mass-

 doi:10.20944/preprints202212.0045.v20

energy equivalence, and time uncertainty with position uncertainty using $\delta t_{\mathrm{HUP}} = \delta R_{\mathrm{HUP}}/c$ [30] yields

$$\delta M_{\mathrm{HUP}} \delta R_{\mathrm{HUP}} \geq \frac{\hbar}{2c}. \tag{A25}$$

Interpreting $\delta M_{\mathrm{HUP}} = \delta R_{\mathrm{HUP}} c^2/(2G)$ as the BH mass in (A25) we derive the Planck length as $\delta R^2_{\mathrm{HUP}} = \ell^2_{\mathrm{P}} \Rightarrow \delta D_{\mathrm{HUP}} = \pm 2\ell_{\mathrm{P}}$ and recover [6] the BH diameter $d_{\mathrm{BH}} = \pm 2$.

However, using the same procedure but inserting the BH radius instead of the BH mass into the uncertainty principle (A25) leads to $\delta M^2_{\mathrm{HUP}} = \frac{1}{4}\hbar c/G = \frac{1}{4}m^2_{\mathrm{P}}$. In general, using the generalized radius (55) in both procedures, we obtain

$$\delta M^2_{\mathrm{HUP}} = \frac{1}{2k} m^2_{\mathrm{P}} \quad \text{and} \quad \delta R^2_{\mathrm{HUP}} = \frac{k}{2}\ell^2_{\mathrm{P}}. \tag{A26}$$

Thus, if k increases, the mass δM_{HUP} decreases, and δR_{HUP} increases and the factor is the same for $k = 1$ i.e., for the *orbital speed radius* $\delta R = G\delta M/c^2$ or *orbital speed mass* $\delta M = \delta R c^2/G$.

Appendix F. Other Definitions of Complex Energies

Let us define the mass/charge energies (61), (62) with different speeds of light, i.e., the charge part of the energy E_{MQ_i} with c_- and the charge part of the energy E_{QM_i} with c_+

$$\begin{aligned}
\tilde{E}_{MQ_i} &:= M_+ c_+^2 + \frac{Q_i}{2\sqrt{\pi\epsilon_0 G}} c_-^2 = m_+ m_{P+} c_+^2 + iq\sqrt{\alpha_+} m_{P+} \frac{\alpha_+^2}{\alpha_-^2} c_+^2 = \left(m_+ + iq\sqrt{\alpha_+}\frac{\alpha_+^2}{\alpha_-^2} \right) E_{P+}, \\
\tilde{E}_{QM_i} &:= \frac{Q}{2\sqrt{\pi\epsilon_0 G}} c_+^2 + M_- c_-^2 = q\sqrt{\alpha_+} m_{P+} c_+^2 + m_- m_{P+} \sqrt{\frac{\alpha_+}{\alpha_-}} \frac{\alpha_+^2}{\alpha_-^2} c_+^2 = \left(q\sqrt{\alpha_+} + m_- \sqrt{\frac{\alpha_+^5}{\alpha_-^5}} \right) E_{P+},
\end{aligned} \tag{A27}$$

If we assume that their squared moduli are equal then

$$m_- = \pm \sqrt{\frac{\alpha_-^5}{\alpha_+^5} \left[q^2 \alpha_+ \left(1 - \frac{\alpha_+^4}{\alpha_-^4} \right) - m_+^2 \right]}, \tag{A28}$$

leads to a type mismatch since $m_+ \in \mathbb{R}$ and $|q|\sqrt{\alpha_+ \left(1 - \alpha_+^4/\alpha_-^4\right)} \in \mathbb{I}$. The same category error would be obtained if E_{MQ_i} was parameterized with c_- and E_{QM_i} with c_+. Therefore, both parts of the complex energy E_{MQ_i} (61) must be expressed by c_+, while both parts of the complex energy E_{QM_i} (62) - by c_-.

Appendix G. Hall Effect

The fractional quantum Hall (FQHE) effect shows a stepwise dependence of the conductance on the magnetic field (as compared to the linear dependence of the Hall effect) with steps quantized as

$$R = \frac{h}{\nu e^2} = \frac{1}{2\nu\epsilon_0 \alpha_* c_*}, \tag{A29}$$

where ν is an integer or fraction (for example, for $\nu = 5/2$, $R = 1/(5\epsilon_0 \alpha c)$). The relations (A29) and (33) suggest that the 2D FQHE links real and imaginary Planck units, similar to 2D graphene, establishing the complementary fine-structure constants.

References

1. de Chardin, P.T. *The Phenomenon of Man*; Harper, New York, 1959.
2. Prigogine, I.; Stengers, I. *Order out of Chaos: Man's New Dialogue with Nature*; Bantam Books, 1984.

3. Melamede, R. Dissipative Structures and the Origins of Life. Unifying Themes in Complex Systems IV; Minai, A.A.; Bar-Yam, Y., Eds.; Springer Berlin Heidelberg: Berlin, Heidelberg, 2008; pp. 80–87.
4. Vedral, V. *Decoding Reality: The Universe as Quantum Information*; Oxford University Press, 2010. doi:https://doi.org/10.1093/oso/9780198815433.001.0001.
5. Łukaszyk, S. Life as the Explanation of the Measurement Problem. *Journal of Physics: Conference Series* **2024**, *2701*, 012124. doi:10.1088/1742-6596/2701/1/012124.
6. Łukaszyk, S., Black Hole Horizons as Patternless Binary Messages and Markers of Dimensionality. In *Future Relativity, Gravitation, Cosmology*; Nova Science Publishers, 2023; chapter 15, pp. 317–374. doi:10.52305/RLIT5885.
7. Vopson, M.M.; Lepadatu, S. Second law of information dynamics. *AIP Advances* **2022**, *12*, 075310. doi:10.1063/5.0100358.
8. Sharma, A.; Czégel, D.; Lachmann, M.; Kempes, C.P.; Walker, S.I.; Cronin, L. Assembly theory explains and quantifies selection and evolution. *Nature* **2023**, *622*, 321–328. doi:10.1038/s41586-023-06600-9.
9. Łukaszyk, S.; Bieniawski, W. Assembly Theory of Binary Messages. *Mathematics* **2024**, *12*, 1600. doi:10.3390/math12101600.
10. Walker, S.I. *Life as no one knows it: The physics of life's emergence*; Riverhead Books: New York, 2024.
11. Platonic Solids in All Dimensions, 2020.
12. Taubes, C.H. Gauge theory on asymptotically periodic {4}-manifolds. *Journal of Differential Geometry* **1987**, *25*. doi:10.4310/jdg/1214440981.
13. Łukaszyk, S. Four Cubes, 2021. arXiv:2007.03782 [math].
14. Lukaszyk, S. Solving the black hole information paradox. *Research Outreach* **2023**. doi:10.32907/RO-134-3956621492.
15. Brukner, Č. A No-Go Theorem for Observer-Independent Facts. *Entropy* **2018**, *20*. doi:10.3390/e20050350.
16. Łukaszyk, S. Novel Recurrence Relations for Volumes and Surfaces of n-Balls, Regular n-Simplices, and n-Orthoplices in Real Dimensions. *Mathematics* **2022**, *10*, 2212. doi:10.3390/math10132212.
17. Łukaszyk, S.; Tomski, A. Omnidimensional Convex Polytopes. *Symmetry* **2023**, *15*. doi:10.3390/sym15030755.
18. Planck, M. Über irreversible Strahlungsvorgänge, 1899.
19. Stoney, G.J. LII. *On the physical units of nature*. *The London, Edinburgh, and Dublin Philosophical Magazine and Journal of Science* **1881**, *11*, 381–390. doi:10.1080/14786448108627031.
20. Kuzmenko, A.B.; van Heumen, E.; Carbone, F.; van der Marel, D. Universal dynamical conductance in graphite. *Physical Review Letters* **2008**, *100*, 117401. arXiv:0712.0835 [cond-mat], doi:10.1103/PhysRevLett.100.117401.
21. Mak, K.F.; Sfeir, M.Y.; Wu, Y.; Lui, C.H.; Misewich, J.A.; Heinz, T.F. Measurement of the Optical Conductivity of Graphene. *Physical Review Letters* **2008**, *101*, 196405. doi:10.1103/PhysRevLett.101.196405.
22. Nair, R.R.; Blake, P.; Grigorenko, A.N.; Novoselov, K.S.; Booth, T.J.; Stauber, T.; Peres, N.M.R.; Geim, A.K. Universal Dynamic Conductivity and Quantized Visible Opacity of Suspended Graphene. *Science* **2008**, *320*, 1308–1308. arXiv:0803.3718 [cond-mat], doi:10.1126/science.1156965.
23. Stauber, T.; Peres, N.M.R.; Geim, A.K. Optical conductivity of graphene in the visible region of the spectrum. *Physical Review B* **2008**, *78*, 085432. doi:10.1103/PhysRevB.78.085432.
24. Wang, X.; Chen, B. Origin of Fresnel problem of two dimensional materials. *Scientific Reports* **2019**, *9*, 17825. doi:10.1038/s41598-019-54338-0.
25. Merano, M. Fresnel coefficients of a two-dimensional atomic crystal. *Physical Review A* **2016**, *93*, 013832. doi:10.1103/PhysRevA.93.013832.
26. Ando, T.; Zheng, Y.; Suzuura, H. Dynamical Conductivity and Zero-Mode Anomaly in Honeycomb Lattices. *Journal of the Physical Society of Japan* **2002**, *71*, 1318–1324. doi:10.1143/JPSJ.71.1318.
27. Zhu, S.E.; Yuan, S.; Janssen, G.C.A.M. Optical transmittance of multilayer graphene. *EPL (Europhysics Letters)* **2014**, *108*, 17007. doi:10.1209/0295-5075/108/17007.
28. Ivanov, I.G.; Hassan, J.U.; Iakimov, T.; Zakharov, A.A.; Yakimova, R.; Janzén, E. Layer-number determination in graphene on SiC by reflectance mapping. *Carbon* **2014**, *77*, 492–500. doi:10.1016/j.carbon.2014.05.054.
29. Varlaki, P.; Nadai, L.; Bokor, J. Number Archetypes in System Realization Theory Concerning the Fine Structure Constant. 2008 International Conference on Intelligent Engineering Systems; IEEE: Miami, FL, 2008; pp. 83–92. doi:10.1109/INES.2008.4481274.
30. Scardigli, F. Some heuristic semi-classical derivations of the Planck length, the Hawking effect and the Unruh effect. *Il Nuovo Cimento B (1971-1996)* **1995**, *110*, 1029–1034. doi:https://doi.org/10.1007/BF02726152.

31. Haug, E.G. Finding the Planck length multiplied by the speed of light without any knowledge of G, c, or h, using a Newton force spring. *Journal of Physics Communications* **2020**, *4*, 075001. doi:10.1088/2399-6528/ab9dd7.
32. Verlinde, E. On the origin of gravity and the laws of Newton. *Journal of High Energy Physics* **2011**, *2011*, 29. doi:10.1007/JHEP04(2011)029.
33. Chung, Y.; Kim, M.; Kim, Y.; Cha, S.; Park, J.W.; Park, J.; Yi, Y.; Song, D.; Ryu, J.H.; Lee, K.; Kim, T.K.; Cacho, C.; Denlinger, J.; Jozwiak, C.; Rotenberg, E.; Bostwick, A.; Kim, K.S. Dark states of electrons in a quantum system with two pairs of sublattices. *Nature Physics* **2024**. doi:10.1038/s41567-024-02586-x.
34. Schneider, L.; Ton, K.T.; Ioannidis, I.; Neuhaus-Steinmetz, J.; Posske, T.; Wiesendanger, R.; Wiebe, J. Proximity superconductivity in atom-by-atom crafted quantum dots. *Nature* **2023**. doi:10.1038/s41586-023-06312-0.
35. Hiller, R.; Putterman, S.J.; Barber, B.P. Spectrum of synchronous picosecond sonoluminescence. *Physical Review Letters* **1992**, *69*, 1182–1184. doi:10.1103/PhysRevLett.69.1182.
36. Eberlein, C. Theory of quantum radiation observed as sonoluminescence. *Physical Review A* **1996**, *53*, 2772–2787. doi:10.1103/PhysRevA.53.2772.
37. Lohse, D.; Schmitz, B.; Versluis, M. Snapping shrimp make flashing bubbles. *Nature* **2001**, *413*, 477–478. doi:10.1038/35097152.
38. Rietman, E.A.; Melcher, B.; Bobrick, A.; Martire, G. A Cylindrical Optical-Space Black Hole Induced from High-Pressure Acoustics in a Dense Fluid. *Universe* **2023**, *9*, 162. doi:10.3390/universe9040162.
39. Melia, F. A Candid Assessment of Standard Cosmology. *Publications of the Astronomical Society of the Pacific* **2022**, *134*, 121001. doi:10.1088/1538-3873/aca51f.
40. Boylan-Kolchin, M. Stress testing ΛCDM with high-redshift galaxy candidates. *Nature Astronomy* **2023**. doi:10.1038/s41550-023-01937-7.
41. Mortlock, D.J.; Warren, S.J.; Venemans, B.P.; Patel, M.; Hewett, P.C.; McMahon, R.G.; Simpson, C.; Theuns, T.; Gonzáles-Solares, E.A.; Adamson, A.; Dye, S.; Hambly, N.C.; Hirst, P.; Irwin, M.J.; Kuiper, E.; Lawrence, A.; Röttgering, H.J.A. A luminous quasar at a redshift of z = 7.085. *Nature* **2011**, *474*, 616–619. doi:10.1038/nature10159.
42. Bosman, S.E.I.; Álvarez Márquez, J.; Colina, L.; Walter, F.; Alonso-Herrero, A.; Ward, M.J.; Östlin, G.; Greve, T.R.; Wright, G.; Bik, A.; Boogaard, L.; Caputi, K.; Costantin, L.; Eckart, A.; García-Marín, M.; Gillman, S.; Hjorth, J.; Iani, E.; Ilbert, O.; Jermann, I.; Labiano, A.; Langeroodi, D.; Peißker, F.; Rinaldi, P.; Topinka, M.; Van Der Werf, P.; Güdel, M.; Henning, T.; Lagage, P.O.; Ray, T.P.; Van Dishoeck, E.F.; Vandenbussche, B. A mature quasar at cosmic dawn revealed by JWST rest-frame infrared spectroscopy. *Nature Astronomy* **2024**. doi:10.1038/s41550-024-02273-0.
43. Comerón, S.; Trujillo, I.; Cappellari, M.; Buitrago, F.; Garduño, L.E.; Zaragoza-Cardiel, J.; Zinchenko, I.A.; Lara-López, M.A.; Ferré-Mateu, A.; Dib, S. The massive relic galaxy NGC 1277 is dark matter deficient: From dynamical models of integral-field stellar kinematics out to five effective radii. *Astronomy & Astrophysics* **2023**, *675*, A143. doi:10.1051/0004-6361/202346291.
44. Brouwer, M.M.; others. First test of Verlinde's theory of emergent gravity using weak gravitational lensing measurements. *Monthly Notices of the Royal Astronomical Society* **2017**, *466*, 2547–2559. doi:https://doi.org/10.1093/mnras/stw3192.
45. Schimmoller, A.J.; McCaul, G.; Abele, H.; Bondar, D.I. Decoherence-free entropic gravity: Model and experimental tests. *Physical Review Research* **2021**, *3*, 033065. doi:10.1103/PhysRevResearch.3.033065.
46. Lukaszyk, S. A No-go Theorem for Superposed Actions (Making Schrödinger's Cat Quantum Nonlocal). In *New Frontiers in Physical Science Research Vol. 3*; Purenovic, D.J., Ed.; Book Publisher International (a part of SCIENCEDOMAIN International), 2022; pp. 137–151. arXiv:1801.08537 [quant-ph], doi:10.9734/bpi/nfpsr/v3/17106D.
47. Qian, K.; Wang, K.; Chen, L.; Hou, Z.; Krenn, M.; Zhu, S.; Ma, X.s. Multiphoton non-local quantum interference controlled by an undetected photon. *Nature Communications* **2023**, *14*, 1480. doi:10.1038/s41467-023-37228-y.
48. Xue, P.; Xiao, L.; Ruffolo, G.; Mazzari, A.; Temistocles, T.; Cunha, M.T.; Rabelo, R. Synchronous Observation of Bell Nonlocality and State-Dependent Contextuality. *Physical Review Letters* **2023**, *130*, 040201. doi:10.1103/PhysRevLett.130.040201.
49. Tran, D.M.; Nguyen, V.D.; Ho, L.B.; Nguyen, H.Q. Increased success probability in Hardy's nonlocality: Theory and demonstration. *Phys. Rev. A* **2023**, *107*, 042210. doi:10.1103/PhysRevA.107.042210.

50. Colciaghi, P.; Li, Y.; Treutlein, P.; Zibold, T. Einstein-Podolsky-Rosen Experiment with Two Bose-Einstein Condensates. *Phys. Rev. X* **2023**, *13*, 021031. doi:10.1103/PhysRevX.13.021031.
51. Kreuzgruber, E.; Wagner, R.; Geerits, N.; Lemmel, H.; Sponar, S. Violation of a Leggett-Garg Inequality Using Ideal Negative Measurements in Neutron Interferometry. *Physical Review Letters* **2024**, *132*, 260201. doi:10.1103/PhysRevLett.132.260201.
52. Watanabe, S. *Knowing and Guessing: A Quantitative Study of Inference and Information*; Wiley, 1969.
53. Watanabe, S. Epistemological Relativity. *Annals of the Japan Association for Philosophy of Science* **1986**, *7*, 1–14. doi:10.4288/jafpos1956.7.1.
54. Saeed, I.; Pak, H.K.; Tlusty, T. Quasiparticles, flat bands and the melting of hydrodynamic matter. *Nature Physics* **2023**. doi:10.1038/s41567-022-01893-5.
55. Bekenstein, J.D. Black Holes and Entropy. *Phys. Rev. D* **1973**, *7*, 2333–2346. doi:10.1103/PhysRevD.7.2333.
56. Vincentelli, F.M.; et al.. A shared accretion instability for black holes and neutron stars. *Nature* **2023**, *615*, 45–49. doi:10.1038/s41586-022-05648-3.
57. Valenzuela-Villaseca, V.; Suttle, L.; Suzuki-Vidal, F.; Halliday, J.; Merlini, S.; Russell, D.; Tubman, E.; Hare, J.; Chittenden, J.; Koepke, M.; Blackman, E.; Lebedev, S. Characterization of Quasi-Keplerian, Differentially Rotating, Free-Boundary Laboratory Plasmas. *Physical Review Letters* **2023**, *130*, 195101. doi:10.1103/PhysRevLett.130.195101.
58. Chaitin, G.J. On the Length of Programs for Computing Finite Binary Sequences. *J. ACM* **1966**, *13*, 547–569. doi:10.1145/321356.321363.
59. Hawking, S. Black hole explosions? *Nature* **1974**, *248*, 30–31. doi:https://doi.org/10.1038/248030a0.
60. Alsing, P.M.; Milburn, G.J. Teleportation with a Uniformly Accelerated Partner. *Phys. Rev. Lett.* **2003**, *91*, 180404. doi:10.1103/PhysRevLett.91.180404.
61. Hooft, G.t. Dimensional Reduction in Quantum Gravity, 1993. doi:10.48550/ARXIV.GR-QC/9310026.
62. Gould, A. Classical derivation of black-hole entropy. *Physical Review D* **1987**, *35*, 449–454. doi:10.1103/PhysRevD.35.449.
63. Penrose, R.; Floyd, R.M. Extraction of Rotational Energy from a Black Hole. *Nature Physical Science* **1971**, *229*, 177–179. doi:10.1038/physci229177a0.
64. Christodoulou, D.; Ruffini, R. Reversible Transformations of a Charged Black Hole. *Physical Review D* **1971**, *4*, 3552–3555. doi:10.1103/PhysRevD.4.3552.
65. Stuchlík, Z.; Kološ, M.; Tursunov, A. Penrose Process: Its Variants and Astrophysical Applications. *Universe* **2021**, *7*, 416. doi:10.3390/universe7110416.
66. Zhang, T. Electric Charge as a Form of Imaginary Energy, 2008.
67. Anderson, E.K.; Baker, C.J.; Bertsche, W.; Bhatt, N.M.; Bonomi, G.; Capra, A.; Carli, I.; Cesar, C.L.; Charlton, M.; Christensen, A.; Collister, R.; Cridland Mathad, A.; Duque Quiceno, D.; Eriksson, S.; Evans, A.; Evetts, N.; Fabbri, S.; Fajans, J.; Ferwerda, A.; Friesen, T.; Fujiwara, M.C.; Gill, D.R.; Golino, L.M.; Gomes Gonçalves, M.B.; Grandemange, P.; Granum, P.; Hangst, J.S.; Hayden, M.E.; Hodgkinson, D.; Hunter, E.D.; Isaac, C.A.; Jimenez, A.J.U.; Johnson, M.A.; Jones, J.M.; Jones, S.A.; Jonsell, S.; Khramov, A.; Madsen, N.; Martin, L.; Massacret, N.; Maxwell, D.; McKenna, J.T.K.; Menary, S.; Momose, T.; Mostamand, M.; Mullan, P.S.; Nauta, J.; Olchanski, K.; Oliveira, A.N.; Peszka, J.; Powell, A.; Rasmussen, C.; Robicheaux, F.; Sacramento, R.L.; Sameed, M.; Sarid, E.; Schoonwater, J.; Silveira, D.M.; Singh, J.; Smith, G.; So, C.; Stracka, S.; Stutter, G.; Tharp, T.D.; Thompson, K.A.; Thompson, R.I.; Thorpe-Woods, E.; Torkzaban, C.; Urioni, M.; Woosaree, P.; Wurtele, J.S. Observation of the effect of gravity on the motion of antimatter. *Nature* **2023**, *621*, 716–722. doi:10.1038/s41586-023-06527-1.
68. Mandelstam, L.; Tamm, I. The Uncertainty Relation Between Energy and Time in Non-relativistic Quantum Mechanics. *J. Phys. (USSR)* **1945**, *9*, 249—-254.
69. Margolus, N.; Levitin, L.B. The maximum speed of dynamical evolution. *Physica D: Nonlinear Phenomena* **1998**, *120*, 188–195. doi:10.1016/S0167-2789(98)00054-2.
70. Levitin, L.B.; Toffoli, T. Fundamental Limit on the Rate of Quantum Dynamics: The Unified Bound Is Tight. *Physical Review Letters* **2009**, *103*, 160502. doi:10.1103/PhysRevLett.103.160502.
71. Iyer, B.R.; Vishveshwara, C.V.; Dhurandhar, S.V. Ultracompact (R<3 M) objects in general relativity. *Classical and Quantum Gravity* **1985**, *2*, 219–228. doi:10.1088/0264-9381/2/2/013.
72. Nemiroff, R.J.; Becker, P.A.; Wood, K.S. Properties of ultracompact neutron stars. *The Astrophysical Journal* **1993**, *406*, 590. doi:10.1086/172471.

73. Lightman, A.P.; Press, W.H.; Price, R.H.; Teukolsky, S.A. *Problem Book in Relativity and Gravitation*; Princeton University Press, 2017. doi:10.2307/j.ctvc774vf.
74. Weinberg, S. *Gravitation and cosmology: Principles and applications of the general theory of relativity*; Wiley: New York, 1972.
75. Morris, M.S.; Thorne, K.S. Wormholes in spacetime and their use for interstellar travel: A tool for teaching general relativity. *American Journal of Physics* **1988**, *56*, 395–412. doi:10.1119/1.15620.
76. Pechenick, K.R.; Ftaclas, C.; Cohen, J.M. Hot spots on neutron stars - The near-field gravitational lens. *The Astrophysical Journal* **1983**, *274*, 846. doi:10.1086/161498.
77. The Event Horizon Telescope Collaboration. First M87 Event Horizon Telescope Results. I. The Shadow of the Supermassive Black Hole. *The Astrophysical Journal Letters* **2019**, *875*, L1. doi:10.3847/2041-8213/ab0ec7.
78. Montgomery, C.; Orchiston, W.; Whittingham, I. Michell, Laplace and the Origin of the Black Hole Concept. *Journal of Astronomical History and Heritage* **2009**, *12*, 90–96. doi:10.3724/SP.J.1440-2807.2009.02.01.
79. Szostek, K.; Szostek, R. The derivation of the general form of kinematics with the universal reference system. *Results in Physics* **2018**, *8*, 429–437. doi:10.1016/j.rinp.2017.12.053.
80. Szostek, R. The Original Method of Deriving Transformations for Kinematics with a Universal Reference System. *Jurnal Fizik Malaysia* **2022**, *43*, 10244–10263.
81. Szostek, R.; Szostek, K. The Existence of a Universal Frame of Reference, in Which it Propagates Light, is Still an Unresolved Problem of Physics. *Jordan Journal of Physics* **2022**, *15*, 457–467. doi:10.47011/15.5.3.
82. Szostek, R. Explanation of What Time in Kinematics Is and Dispelling Myths Allegedly Stemming from the Special Theory of Relativity. *Applied Sciences* **2022**, *12*, 6272. doi:10.3390/app12126272.
83. Unnikrishnan, C.S. Cosmic Gravity and the Quantum Spin. In *New Relativity in the Gravitational Universe*; Springer International Publishing: Cham, 2022; Vol. 209, pp. 373–405. doi:10.1007/978-3-031-08935-0_13.
84. Unnikrishnan, C.S. Cosmic Relativity—The Theory and Its Primary Fundamental Results. In *New Relativity in the Gravitational Universe*; Springer International Publishing: Cham, 2022; Vol. 209, pp. 255–306. doi:10.1007/978-3-031-08935-0_10.
85. Szostek, Karol and Szostek, Roman. The concept of a mechanical system for measuring the one-way speed of light. *Technical Transactions* **2023**, *2023*, 1–9. doi:10.37705/TechTrans/e2023003.
86. Event Horizon Telescope Collaboration.; Akiyama, K.; Alberdi, A.; Alef, W.; Algaba, J.C.; Anantua, R.; Asada, K.; Azulay, R.; Bach, U.; Baczko, A.K.; Ball, D.; Baloković, M.; Barrett, J.; Bauböck, M.; Benson, B.A.; Bintley, D.; Blackburn, L.; Blundell, R.; Bouman, K.L.; Bower, G.C.; Boyce, H.; Bremer, M.; Brinkerink, C.D.; Brissenden, R.; Britzen, S.; Broderick, A.E.; Broguiere, D.; Bronzwaer, T.; Bustamante, S.; Byun, D.Y.; Carlstrom, J.E.; Ceccobello, C.; Chael, A.; Chan, C.k.; Chatterjee, K.; Chatterjee, S.; Chen, M.T.; Chen, Y.; Cheng, X.; Cho, I.; Christian, P.; Conroy, N.S.; Conway, J.E.; Cordes, J.M.; Crawford, T.M.; Crew, G.B.; Cruz-Osorio, A.; Cui, Y.; Davelaar, J.; Laurentis, M.D.; Deane, R.; Dempsey, J.; Desvignes, G.; Dexter, J.; Dhruv, V.; Doeleman, S.S.; Dougal, S.; Dzib, S.A.; Eatough, R.P.; Emami, R.; Falcke, H.; Farah, J.; Fish, V.L.; Fomalont, E.; Ford, H.A.; Fraga-Encinas, R.; Freeman, W.T.; Friberg, P.; Fromm, C.M.; Fuentes, A.; Galison, P.; Gammie, C.F.; García, R.; Gentaz, O.; Georgiev, B.; Goddi, C.; Gold, R.; Gómez-Ruiz, A.I.; Gómez, J.L.; Gu, M.; Gurwell, M.; Hada, K.; Haggard, D.; Haworth, K.; Hecht, M.H.; Hesper, R.; Heumann, D.; Ho, L.C.; Ho, P.; Honma, M.; Huang, C.W.L.; Huang, L.; Hughes, D.H.; Ikeda, S.; Impellizzeri, C.M.V.; Inoue, M.; Issaoun, S.; James, D.J.; Jannuzi, B.T.; Janssen, M.; Jeter, B.; Jiang, W.; Jiménez-Rosales, A.; Johnson, M.D.; Jorstad, S.; Joshi, A.V.; Jung, T.; Karami, M.; Karuppusamy, R.; Kawashima, T.; Keating, G.K.; Kettenis, M.; Kim, D.J.; Kim, J.Y.; Kim, J.; Kim, J.; Kino, M.; Koay, J.Y.; Kocherlakota, P.; Kofuji, Y.; Koch, P.M.; Koyama, S.; Kramer, C.; Kramer, M.; Krichbaum, T.P.; Kuo, C.Y.; Bella, N.L.; Lauer, T.R.; Lee, D.; Lee, S.S.; Leung, P.K.; Levis, A.; Li, Z.; Lico, R.; Lindahl, G.; Lindqvist, M.; Lisakov, M.; Liu, J.; Liu, K.; Liuzzo, E.; Lo, W.P.; Lobanov, A.P.; Loinard, L.; Lonsdale, C.J.; Lu, R.S.; Mao, J.; Marchili, N.; Markoff, S.; Marrone, D.P.; Marscher, A.P.; Martí-Vidal, I.; Matsushita, S.; Matthews, L.D.; Medeiros, L.; Menten, K.M.; Michalik, D.; Mizuno, I.; Mizuno, Y.; Moran, J.M.; Moriyama, K.; Moscibrodzka, M.; Müller, C.; Mus, A.; Musoke, G.; Myserlis, I.; Nadolski, A.; Nagai, H.; Nagar, N.M.; Nakamura, M.; Narayan, R.; Narayanan, G.; Natarajan, I.; Nathanail, A.; Fuentes, S.N.; Neilsen, J.; Neri, R.; Ni, C.; Noutsos, A.; Nowak, M.A.; Oh, J.; Okino, H.; Olivares, H.; Ortiz-León, G.N.; Oyama, T.; Özel, F.; Palumbo, D.C.M.; Paraschos, G.F.; Park, J.; Parsons, H.; Patel, N.; Pen, U.L.; Pesce, D.W.; Piétu, V.; Plambeck, R.; PopStefanija, A.; Porth, O.; Pötzl, F.M.; Prather, B.; Preciado-López, J.A.; Psaltis, D.; Pu, H.Y.; Ramakrishnan, V.; Rao, R.; Rawlings, M.G.; Raymond, A.W.; Rezzolla, L.; Ricarte, A.; Ripperda, B.; Roelofs, F.; Rogers, A.; Ros, E.; Romero-Cañizales, C.; Roshanineshat, A.; Rottmann, H.;

 doi:10.20944/preprints202212.0045.v20

Roy, A.L.; Ruiz, I.; Ruszczyk, C.; Rygl, K.L.J.; Sánchez, S.; Sánchez-Argüelles, D.; Sánchez-Portal, M.; Sasada, M.; Satapathy, K.; Savolainen, T.; Schloerb, F.P.; Schonfeld, J.; Schuster, K.F.; Shao, L.; Shen, Z.; Small, D.; Sohn, B.W.; SooHoo, J.; Souccar, K.; Sun, H.; Tazaki, F.; Tetarenko, A.J.; Tiede, P.; Tilanus, R.P.J.; Titus, M.; Torne, P.; Traianou, E.; Trent, T.; Trippe, S.; Turk, M.; Van Bemmel, I.; Van Langevelde, H.J.; Van Rossum, D.R.; Vos, J.; Wagner, J.; Ward-Thompson, D.; Wardle, J.; Weintroub, J.; Wex, N.; Wharton, R.; Wielgus, M.; Wiik, K.; Witzel, G.; Wondrak, M.F.; Wong, G.N.; Wu, Q.; Yamaguchi, P.; Yoon, D.; Young, A.; Young, K.; Younsi, Z.; Yuan, F.; Yuan, Y.F.; Zensus, J.A.; Zhang, S.; Zhao, G.Y.; Zhao, S.S.; Agurto, C.; Allardi, A.; Amestica, R.; Araneda, J.P.; Arriagada, O.; Berghuis, J.L.; Bertarini, A.; Berthold, R.; Blanchard, J.; Brown, K.; Cárdenas, M.; Cantzler, M.; Caro, P.; Castillo-Domínguez, E.; Chan, T.L.; Chang, C.C.; Chang, D.O.; Chang, S.H.; Chang, S.C.; Chen, C.C.; Chilson, R.; Chuter, T.C.; Ciechanowicz, M.; Colin-Beltran, E.; Coulson, I.M.; Crowley, J.; Degenaar, N.; Dornbusch, S.; Durán, C.A.; Everett, W.B.; Faber, A.; Forster, K.; Fuchs, M.M.; Gale, D.M.; Geertsema, G.; González, E.; Graham, D.; Gueth, F.; Halverson, N.W.; Han, C.C.; Han, K.C.; Hasegawa, Y.; Hernández-Rebollar, J.L.; Herrera, C.; Herrero-Illana, R.; Heyminck, S.; Hirota, A.; Hoge, J.; Hostler Schimpf, S.R.; Howie, R.E.; Huang, Y.D.; Jiang, H.; Jinchi, H.; John, D.; Kimura, K.; Klein, T.; Kubo, D.; Kuroda, J.; Kwon, C.; Lacasse, R.; Laing, R.; Leitch, E.M.; Li, C.T.; Liu, C.T.; Liu, K.Y.; Lin, L.C.C.; Lu, L.M.; Mac-Auliffe, F.; Martin-Cocher, P.; Matulonis, C.; Maute, J.K.; Messias, H.; Meyer-Zhao, Z.; Montaña, A.; Montenegro-Montes, F.; Montgomerie, W.; Moreno Nolasco, M.E.; Muders, D.; Nishioka, H.; Norton, T.J.; Nystrom, G.; Ogawa, H.; Olivares, R.; Oshiro, P.; Pérez-Beaupuits, J.P.; Parra, R.; Phillips, N.M.; Poirier, M.; Pradel, N.; Qiu, R.; Raffin, P.A.; Rahlin, A.S.; Ramírez, J.; Ressler, S.; Reynolds, M.; Rodríguez-Montoya, I.; Saez-Madain, A.F.; Santana, J.; Shaw, P.; Shirkey, L.E.; Silva, K.M.; Snow, W.; Sousa, D.; Sridharan, T.K.; Stahm, W.; Stark, A.A.; Test, J.; Torstensson, K.; Venegas, P.; Walther, C.; Wei, T.S.; White, C.; Wieching, G.; Wijnands, R.; Wouterloot, J.G.A.; Yu, C.Y.; Yu, W.; Zeballos, M. First Sagittarius A* Event Horizon Telescope Results. I. The Shadow of the Supermassive Black Hole in the Center of the Milky Way. *The Astrophysical Journal Letters* **2022**, *930*, L12. doi:10.3847/2041-8213/ac6674.

87. Broderick, A.E.; Pesce, D.W.; Gold, R.; Tiede, P.; Pu, H.Y.; Anantua, R.; Britzen, S.; Ceccobello, C.; Chatterjee, K.; Chen, Y.; Conroy, N.S.; Crew, G.B.; Cruz-Osorio, A.; Cui, Y.; Doeleman, S.S.; Emami, R.; Farah, J.; Fromm, C.M.; Galison, P.; Georgiev, B.; Ho, L.C.; James, D.J.; Jeter, B.; Jimenez-Rosales, A.; Koay, J.Y.; Kramer, C.; Krichbaum, T.P.; Lee, S.S.; Lindqvist, M.; Martí-Vidal, I.; Menten, K.M.; Mizuno, Y.; Moran, J.M.; Moscibrodzka, M.; Nathanail, A.; Neilsen, J.; Ni, C.; Park, J.; Piétu, V.; Rezzolla, L.; Ricarte, A.; Ripperda, B.; Shao, L.; Tazaki, F.; Toma, K.; Torne, P.; Weintroub, J.; Wielgus, M.; Yuan, F.; Zhao, S.S.; Zhang, S. The Photon Ring in M87*. *The Astrophysical Journal* **2022**, *935*, 61. doi:10.3847/1538-4357/ac7c1d.
88. Johnson, M.D.; Lupsasca, A.; Strominger, A.; Wong, G.N.; Hadar, S.; Kapec, D.; Narayan, R.; Chael, A.; Gammie, C.F.; Galison, P.; Palumbo, D.C.M.; Doeleman, S.S.; Blackburn, L.; Wielgus, M.; Pesce, D.W.; Farah, J.R.; Moran, J.M. Universal interferometric signatures of a black hole's photon ring. *Science Advances* **2020**, *6*, eaaz1310. doi:10.1126/sciadv.aaz1310.
89. Conover, E. Physicists dispute a claim of detecting a black hole's 'photon ring', 2022.
90. Gralla, S.E.; Lupsasca, A.; Marrone, D.P. The shape of the black hole photon ring: A precise test of strong-field general relativity. *Physical Review D* **2020**, *102*, 124004. doi:10.1103/PhysRevD.102.124004.
91. Lockhart, W.; Gralla, S.E. How narrow is the M87* ring – II. A new geometric model. *Monthly Notices of the Royal Astronomical Society* **2022**, *517*, 2462–2470. doi:10.1093/mnras/stac2743.
92. Tiede, P.; Johnson, M.D.; Pesce, D.W.; Palumbo, D.C.M.; Chang, D.O.; Galison, P. Measuring Photon Rings with the ngEHT. *Galaxies* **2022**, *10*, 111. doi:10.3390/galaxies10060111.
93. Cárdenas-Avendaño, A.; Lupsasca, A. Prediction for the interferometric shape of the first black hole photon ring. *Physical Review D* **2023**, *108*, 064043. doi:10.1103/PhysRevD.108.064043.
94. Chen, X.H.; Li, A.; Zhang, K. On Graphene in the Interstellar Medium. *The Astrophysical Journal* **2017**, *850*, 104. doi:10.3847/1538-4357/aa93d5.
95. Zhang, W.; Liang, Q.; Li, X.; Ma, L.P.; Li, X.; Zhao, Z.; Zhang, R.; Cao, H.; Wang, Z.; Li, W.; Wang, Y.; Liu, M.; Yue, N.; Liu, H.; Hu, Z.; Liu, L.; Zhou, Q.; Li, F.; Zheng, W.; Ren, W.; Zou, M. Discovery of natural few-layer graphene on the Moon. *National Science Review* **2024**, p. nwae211. doi:10.1093/nsr/nwae211.
96. Abbott, B.P.; et al.. GW170817: Observation of Gravitational Waves from a Binary Neutron Star Inspiral. *Physical Review Letters* **2017**, *119*, 161101. doi:10.1103/PhysRevLett.119.161101.

97. Szostek, R.; Góralski, P.; Szostek, K. Gravitational waves in Newton's gravitation and criticism of gravitational waves resulting from the General Theory of Relativity (LIGO). *Bulletin of the Karaganda University. "Physics" Series* **2019**, *96*, 39–56. doi:10.31489/2019Ph4/39-56.
98. Chojnacki, L.; Pohle, R.; Yan, H.; Akagi, Y.; Shannon, N. Gravitational wave analogs in spin nematics and cold atoms. *Physical Review B* **2024**, *109*, L220407. doi:10.1103/PhysRevB.109.L220407.
99. Hawking, S.W., Ed. *Three hundred years of gravitation*, transferred to digital print ed.; Cambridge University Press: Cambridge, 2003.
100. Kalogera, V.; Baym, G. The Maximum Mass of a Neutron Star. *The Astrophysical Journal* **1996**, *470*, L61–L64. doi:10.1086/310296.
101. Ai, S.; Gao, H.; Zhang, B. What Constraints on the Neutron Star Maximum Mass Can One Pose from GW170817 Observations? *The Astrophysical Journal* **2020**, *893*, 146. doi:10.3847/1538-4357/ab80bd.
102. Wurdack, M.; Yun, T.; Katzer, M.; Truscott, A.G.; Knorr, A.; Selig, M.; Ostrovskaya, E.A.; Estrecho, E. Negative-mass exciton polaritons induced by dissipative light-matter coupling in an atomically thin semiconductor. *Nature Communications* **2023**, *14*, 1026. doi:10.1038/s41467-023-36618-6.
103. Moroianu, A.; Wen, L.; James, C.W.; Ai, S.; Kovalam, M.; Panther, F.H.; Zhang, B. An assessment of the association between a fast radio burst and binary neutron star merger. *Nature Astronomy* **2023**. doi:10.1038/s41550-023-01917-x.
104. Lai, D. IXPE detection of polarized X-rays from magnetars and photon mode conversion at QED vacuum resonance. *Proceedings of the National Academy of Sciences* **2023**, *120*, e2216534120. doi:10.1073/pnas.2216534120.
105. Anna-Thomas, R.; Connor, L.; Dai, S.; Feng, Y.; Burke-Spolaor, S.; Beniamini, P.; Yang, Y.P.; Zhang, Y.K.; Aggarwal, K.; Law, C.J.; Li, D.; Niu, C.; Chatterjee, S.; Cruces, M.; Duan, R.; Filipovic, M.D.; Hobbs, G.; Lynch, R.S.; Miao, C.; Niu, J.; Ocker, S.K.; Tsai, C.W.; Wang, P.; Xue, M.; Yao, J.M.; Yu, W.; Zhang, B.; Zhang, L.; Zhu, S.; Zhu, W. Magnetic field reversal in the turbulent environment around a repeating fast radio burst. *Science* **2023**, *380*, 599–603. doi:10.1126/science.abo6526.
106. Li, D.; Wagle, P.; Chen, Y.; Yunes, N. Perturbations of Spinning Black Holes beyond General Relativity: Modified Teukolsky Equation. *Physical Review X* **2023**, *13*, 021029. doi:10.1103/PhysRevX.13.021029.
107. Sneppen, A.; Watson, D.; Bauswein, A.; Just, O.; Kotak, R.; Nakar, E.; Poznanski, D.; Sim, S. Spherical symmetry in the kilonova AT2017gfo/GW170817. *Nature* **2023**, *614*, 436–439. doi:10.1038/s41586-022-05616-x.
108. Susskind, L. *Black Hole War: My Battle with Stephen Hawking to Make the World Safe for Quantum Mechanics*; Little, Brown and Company, 2008.
109. Peng, X.; Zhou, H.; Wei, B.B.; Cui, J.; Du, J.; Liu, R.B. Experimental Observation of Lee-Yang Zeros. *Physical Review Letters* **2015**, *114*, 010601. doi:10.1103/PhysRevLett.114.010601.
110. Gnatenko, K.; Kargol, A.; Tkachuk, V. Lee–Yang zeros and two-time spin correlation function. *Physica A: Statistical Mechanics and its Applications* **2018**, *509*, 1095–1101. doi:10.1016/j.physa.2018.06.103.
111. Marques Muniz, A.L.; Wu, F.O.; Jung, P.S.; Khajavikhan, M.; Christodoulides, D.N.; Peschel, U. Observation of photon-photon thermodynamic processes under negative optical temperature conditions. *Science* **2023**, *379*, 1019–1023. doi:10.1126/science.ade6523.
112. Wang, S.; Hu, Z.; Wu, Q.; Chen, H.; Prodan, E.; Zhu, R.; Huang, G. Smart patterning for topological pumping of elastic surface waves. *Science Advances* **2023**, *9*, eadh4310. doi:10.1126/sciadv.adh4310.
113. Fidkowski, L.; Hubeny, V.; Kleban, M.; Shenker, S. The Black Hole Singularity in AdS/CFT. *Journal of High Energy Physics* **2004**, *2004*, 014–014. doi:10.1088/1126-6708/2004/02/014.
114. Ali, A.F.; Moulay, E.; Jusufi, K.; Alshal, H. Unitary symmetries in wormhole geometry and its thermodynamics. *The European Physical Journal C* **2022**, *82*, 1170. doi:10.1140/epjc/s10052-022-11095-1.
115. Aksteiner, S.; Araneda, B. Kähler Geometry of Black Holes and Gravitational Instantons. *Physical Review Letters* **2023**, *130*, 161502. doi:10.1103/PhysRevLett.130.161502.
116. Capozziello, S.; De Bianchi, S.; Battista, E. Avoiding singularities in Lorentzian-Euclidean black holes: The role of atemporality. *Physical Review D* **2024**, *109*, 104060. doi:10.1103/PhysRevD.109.104060.
117. Jussila, H.; Yang, H.; Granqvist, N.; Sun, Z. Surface plasmon resonance for characterization of large-area atomic-layer graphene film. *Optica* **2016**, *3*, 151. doi:10.1364/OPTICA.3.000151.
118. Wallace, P.R. Erratum: The Band Theory of Graphite [Phys. Rev. 71, 622 (1947)]. *Physical Review* **1947**, *72*, 258–258. doi:10.1103/PhysRev.72.258.

119. Novoselov, K.S.; Geim, A.K.; Morozov, S.V.; Jiang, D.; Zhang, Y.; Dubonos, S.V.; Grigorieva, I.V.; Firsov, A.A. Electric Field Effect in Atomically Thin Carbon Films. *Science* **2004**, *306*, 666–669. doi:10.1126/science.1102896.
120. Einstein, A.; Podolsky, B.; Rosen, N. Can Quantum-Mechanical Description of Physical Reality Be Considered Complete? *Physical Review* **1935**, *47*, 777–780. doi:10.1103/PhysRev.47.777.
121. Bell, J.S. On the Einstein Podolsky Rosen paradox. *Physics Physique Fizika* **1964**, *1*, 195–200. doi:10.1103/PhysicsPhysiqueFizika.1.195.
122. Łukaszyk, S. A short note about graphene and the fine structure constant, 2020. doi:10.13140/RG.2.2.21718.88641.
123. Łukaszyk, S. A short note about the geometry of graphene, 2020. doi:10.13140/RG.2.2.11500.18569/1.
124. Mahajan, S. Calculation of the pi-like circular constants in curved geometry. ResearchGate, 2013.
125. The 2023 Pole Marker, 2023.
126. Schrinski, B.; Yang, Y.; Von Lüpke, U.; Bild, M.; Chu, Y.; Hornberger, K.; Nimmrichter, S.; Fadel, M. Macroscopic Quantum Test with Bulk Acoustic Wave Resonators. *Physical Review Letters* **2023**, *130*, 133604. doi:10.1103/PhysRevLett.130.133604.
127. Tobar, M.E. Global representation of the fine structure constant and its variation. *Metrologia* **2005**, *42*, 129–133. doi:10.1088/0026-1394/42/2/007.
128. Lin, X.; Du, R.; Xie, X. Recent experimental progress of fractional quantum Hall effect: 5/2 filling state and graphene. *National Science Review* **2014**, *1*, 564–579. doi:10.1093/nsr/nwu071.